

LIBRARY
Michigan State
University

This is to certify that the

dissertation entitled

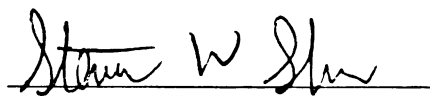
THE DYNAMIC PERFORMANCE OF AN IMPACT PRINT HAMMER
OF THE STORED ENERGY TYPE

presented by

Pi-Cheng Tung

has been accepted towards fulfillment
of the requirements for

Ph.D. degree in Mechanical Engineering


Major professor

Date 9-8-87



RETURNING MATERIALS:

Place in book drop to
remove this checkout from
your record. FINES will
be charged if book is
returned after the date
stamped below.

--	--	--

**THE DYNAMIC PERFORMANCE OF AN IMPACT PRINT HAMMER
OF THE STORED ENERGY TYPE**

By

Pi-Cheng Tung

A DISSERTATION

Submitted to
Michigan State University
in partial fulfilment of the requirements
for the degree of

DOCTOR OF PHILOSOPHY

Department of Mechanical Engineering

1987

ABSTRACT

THE DYNAMIC PERFORMANCE OF AN IMPACT PRINT HAMMER

By

Pi-Cheng Tung

The methods of dynamical systems and bifurcation theories are applied to a mathematical model which is developed to describe the characteristic behavior of an impact print hammer of the stored energy type. The armature of the print hammer is represented by a mass held against a backstop by a preloaded linear spring with negative stiffness which characterizes the net effect of a permanent magnet and a prestressed flexible beam. Periodic half-sine pulses are adopted to represent the effect of currents which oppose the permanent magnet and release the armature to strike the ribbon and paper which is represented by a linear spring and a linear viscous dashpot. A coefficient of restitution is employed to characterize the almost instantaneous behavior of impact and rebound at the backstop.

For periodic inputs to the printer the existence of periodic motions with n impacts at the backstop per forcing cycle is determined using a matching of the solutions in each linear region of the phase space. The stability and bifurcations of these motions are examined using a Poincare map. It is determined that nearly all such periodic motions are unstable. In fact, only a very narrow range of driving

periods admits any stable solutions. This indicates that periodic operation of the printer is not generally feasible.

Chaotic motions, in the form of strange attractors for the Poincare map, are found to exist over wide ranges of driving periods. The existence of Smale horseshoes has been determined in one such case by showing that the stable and unstable manifolds of a saddle type periodic motion intersect transversally. These horseshoes are extremely complicated invariant sets for the map which contain an infinite number of periodic and nonperiodic motions. Lyapunov exponents which measure the average of exponential rates of convergence and divergence of long time trajectories in phase space have also been computed for chaotic motions.

The influence of various parameters on the performance of the model have been considered to determine if the stable operating range can be expanded so as to make periodic printing feasible. It is shown that an increase in the damping at the backstop or an increase in the preload will enhance stability by reducing the settle out time of rebounds at the backstop. They, however, are not sufficient to increase the operating speed appreciably.

The primary limitation on speed is due to uncertainty in the position and velocity of the armature during settle out. This causes variations in flight time and print forces. An open loop control strategy is introduced which modifies the driving pulse such that it aids the restoring force on the armature during settle out. This is achieved by application of a damping pulse, opposite in sense to the driving pulse, immediately before the driving pulse. This is done in an open loop fashion which requires no sensors.

The control method is tested using a set of printer performance criteria, developed in the thesis, which guarantee that acceptable print force will be achieved for arbitrarily timed pulses with some minimum time lapse between them. These criteria are used to show that the modified pulses increase the print speed for both periodic and nonperiodic inputs. The criteria are quite general and may be useful for more complicated models and controllers.

To my parents

ACKNOWLEDGEMENTS

I wish to express my deepest gratitude to my advisor Dr. Steven W Shaw for his guidance and assistance throughout this study and in preparation of this manuscript. His academic excellence and good personality have provided a constant source of encouragement.

Also, I wish to extend my sincere thank to other members of my Doctoral Guidance committee, Dr. Ronald Rosenberg, Hassan Khalil, and Shui-Nee Chow.

This research was financially supported through the effort of Dr. Steven W. Shaw by the National Science Foundation under grants MEA-8421248 AND MSM-8613294 and by DARPA. This support is gratefully acknowledged.

Finally, I would like to thank my family for their loving support.

TABLE OF CONTENTS

LIST OF FIGURES

CHAPTER I. INTRODUCTION	1
1.1 Dot Matrix Impact Printers	1
1.2 Literature Survey	3
1.3 Scope of the Investigation	9
1.4 Dissertation Arrangement	12
 CHAPTER II. MODEL AND METHODS OF ANALYSIS	 14
2.1 Mathematical Model	14
2.2 Methods of Analysis	20
2.3 Bifurcation	29
 CHAPTER III. THE DYNAMIC RESPONSE : PERIODIC INPUT	 34
3.1 Existence of Periodic Motions	34
3.2 Stability Analysis	40
3.3 Simulation and Observations	53
3.4 Chaotic Dynamics of the System	66
 CHAPTER V. A METHOD FOR THE IMPROVEMENT OF PERFORMANCE	 80
4.1 An Open Loop Control Strategy and Printer Performance	80
Criteria	

4.2 Simulations and Results : Periodic Input	89
4.3 Simulations and Results : General Firing Combinations	95
 CHAPTER IV. DISCUSSION AND CONCLUSIONS	 100
 LIST OF REFERENCES	 105

LIST OF FIGURES

Figure		Page
1.	Impact printer of the stored energy type. (duplicated from Figure 1 in [10], with permission).	15
2.	A model of the simplified dynamical system.	15
3.	(a) the phase portrait with single sine pulse excitation, $\beta=3.2$, $\alpha_1=0.005$, $\alpha_2=0.2$, $k=1.56$, $F_0=1.0345$, $D=0.66$, $\delta=0.9$, $\alpha=0.6$, $x_{01}=0.2$, $x_{02}=0.8$, $b=0.15$.	21
	(b) the phase portrait with single sine pulse excitation from Hendriks' model. (duplicated from Figure 10, [10], with permission).	21
4.	The net restoring force versus displacement.	22
5.	The excitation force versus time.	22
6.	(a) phase portrait with single impact per forcing cycle.	23
	(b) phase portrait with two impacts per forcing cycle.	23
7.	(a) a supercritical flip bifurcation.	32
	(b) a subcritical flip bifurcation.	32
8.	A saddle-node bifurcation.	33
9.	Resonance curves \bar{y} versus forcing period T .	39
10.	(a) flip bifurcation curve of forcing period T versus backstop material factor α for $n=1$.	54
	(b) flip bifurcation curve of forcing period T versus system damping α_1 for $n=1$.	54
11.	Flip bifurcation sequence	
	(a) period 1 orbit, $T=3.2$	55
	(b) period 2 orbit, $T=3.45$	55
	(c) period 4 orbit, $T=3.48$	56
	(d) chaotic motion, $T=3.9$	56

12.	Motion shown in Σ , same parameter values as in Figure 11.	58 59
13.	Sequence of Poincare plots at decreasing forcing period T .	60 61
14.	(a) a Poincare plot at a forcing frequency near that of "buzz printing", $T=2.5$ (b) a chaotic motion at a forcing frequency near that of "buzz printing", $T=2.5$. (c) a plot of displacement versus time at a forcing frequency near that of "buzz of printing", $T=2.5$	62 63 63
15.	A plot of settle-out time versus the additional preload	65
16.	A plot of settle-out time versus the backstop material factor α .	65
17.	Frequency response.	69
18.	Intersection of the stable manifold and the unstable manifold.	69
19.	Periodic full sine pulses.	81
20.	General firing combinations with full sine pulses.	84
21.	(a) A driving cycle. (b) Composite map in Σ .	87 87
22.	(a) paper impact velocity versus forcing period for periodic half sine pulses (piecewise linear model). (b) paper impact velocity versus forcing period for periodic full sine pulses (piecewise linear model).	91 91
23.	(a) maximum paper force versus forcing period for periodic half sine pulses (piecewise linear model). (b) maximum paper force versus forcing period for periodic full sine pulses (piecewise linear model).	92 92
24.	(a) paper impact velocity versus forcing period for periodic half sine pulses (Hendriks' model [10]). (b) paper impact velocity versus forcing period for periodic full sine pulses (Hendriks' model [10]).	93 93

25.	(a) maximum paper force versus forcing period for periodic half sine pulses (Hendriks' model [10]).	94
	(b) maximum paper force versus forcing period for periodic full sine pulses (Hendriks' model [10]).	94
26.	Acceptable print region Ω .	96
27.	Initial condition of $P(D) \subset \Omega$, forcing period $T=5.25$	98
28.	Initial condition of $P(D) \subset \Omega$, forcing period $T=5.5$	98

CHAPTER I

INTRODUCTION

1.1 Dot matrix impact printers

Printing technology has been developed during the past thirty years to meet the need of printing large quantities of data at a very high rate of speed and the requirement of high print quality and low cost. Today dot matrix impact printers with the electronic timing and control have become the most common computer hardcopy output device. They offer high printing speed, low cost, and the ability of producing multiple copies. Although non-impact printing technologies such as ink-jet, thermaltransfer and laser are fast developing and can offer the advantages of quiet operation, high-quality resolution, and high-function operation, its hardware costs and reliability cannot yet match those of dot matrix impact printers [1-4].

In dot matrix impact printers, each character is formed on the paper from an array of dots, and each dot is made by driving a wire into a ribbon which transfers ink onto the paper. High speed wire matrix printers usually have a 5x7 array of wires for each print position, and thus are able to print an entire line of characters in parallel. In such a manner characters, pictures, charts and graphs can be generated by the printer. The three most common types of dot matrix impact printers are the stored energy type, tubular or plunger

type, and clapper or relay type. Each has unique characteristics, with associated advantages and disadvantages [5].

In the stored energy type, a permanent magnet holds a prestressed spring member in a cocked position until a dot on the paper is desired. When energized with a current of appropriate sense and magnitude, a coil produces a magnetic field that opposes the field of the permanent magnet and releases the deflected spring. This spring propels the print wire which is attached to the armature, to strike the ribbon and paper. The current in the coil is terminated near the time of impact with the paper. Upon returning from the ribbon and paper, the armature, due to the permanent force, hits the backstop and rebounds against the backstop, damping its motion during settle-out until it is energized again. This type of impact printer has a large force at the initiation of the print cycle which brings the print wire up to print speed very quickly. This printer has the highest potential for high speed printing.

In the plunger type of impact printers, the tubular solenoid has a cylindrical shape with a coil around a central plunger. The plunger is pulled forward when the coil is energized and moves the print wire connected to it. The plunger is returned to its initial position after the wire strikes the ribbon and paper by the rebound from the paper and by a flat spring connected to the end of the plunger.

In clapper type of impact printers, the solenoid consists of a relay mechanism where a clapper (armature) closes an air gap when a coil surrounding part of its core is energized. The moving clapper pushes a print wire against the ribbon and paper. This approach is unique in that the print wire is not attached to its driving spring

member. Instead, the print wire is simply held against the clapper by a small spring which also holds the print wire and clapper in proper position before firing and helps to settle out the bouncing of both after firing. This printer has the advantages of simplicity, low manufacturing cost, long life, and ease of use.

In order to meet market requirement for high speed printing, wire dot print head mechanisms had been changed from plunger type to clapper type. Currently, the stored energy type of printers is very practical owing to the fact that it has a large initial activation force and thus can be operated at higher frequencies [5,6]. Despite the fact that impact printers will be continue to hold a significant position in the printer marketplace, printer actuator mechanisms must become faster, i.e., higher repetition rates for the hammer must be achieved without compromising cost. A study of impact hammer dynamics and the factors which limit their speed would be helpful in meeting these needs.

1.2 Literature Survey

The subject of impact printers has been studied by a number of authors in the past years. Dauer [7] has described the contact time, the time which the hammer is in contact with paper. The contact time plays a key role in reducing the horizontal slur of the characters which occurs when the moving wire comes in contact with the ribbon and paper. In Dauer [7] a hard spring with nonlinear cubic term was adopted to characterize the behavior of a paper pack. With a simple

model the contact time is shown to be inversely proportional to the square root of the initial hammer velocity [7]. Wang and Hall [8] used experimental techniques based on optical measurement to describe the force-deformation characteristic of paper and ribbon in dot matrix impact printing. Maximum paper indentation, peak contact force, and contact time were determined. Watanabe et al. [5] have analyzed the coupling of the longitudinal and the transverse collision vibrations at the paper impact by the wave equation and a new mechanism of wire dot print head of the stored energy type has been proposed. They suggested that the connection point of the armature with the wire be set to be the center of percussion and the spring be connected to the center of rotation of the armature. Such a device can eliminate secondary vibrations, due to the interaction of the armature and the driving spring, which is undesirable. Yang et al. [9] discussed the dynamic impact response and wire guide design of the dot matrix printer head mechanism of the stored energy type. Due to the limitation of print resolution, the slenderness ratio of wires are typically very large. Without the support of a wire guide, good print quality cannot be achieved. In Yang et al. [9] the guide number and guide position are optimally designed by using the general slope deflection method. Also, paper-ribbon deformation and impact stress waves are studied by using a finite element method.

Hendriks [10] has investigated the behavior of the impact printer by considering several nonlinear effects, including the effect due to impacts at the backstop. Using simulations of a simple model, he showed that under repeated excitation the bounce phenomenon of the hammer against the backstop contained high frequency forces and

produced responses of great complexity. He pointed out that at low repetition rates each impact was distinct and essentially independent, but at high repetition rates the impacts interacted, causing print time and force variations and thus unacceptable print quality. This is due to the fact that at low repetition rates there is enough time for nearly complete settle-out of the hammer and the armature essentially returns to the rest position against the backstop, thus allowing the next cycle to proceed without interacting with previous one. However, at high repetition rates, the armature will be fired during the settle-out phase, this provides essentially random initial conditions for subsequent actuations. This is the limiting factor in the operating speed of these printers.

A survey report by Hall [11] about works related to the improvement of impact printer performance indicated that there are only a few works [12-16] related to the impact printer of dot matrix type, and all are patents.

There are some published works related to the increasing of the operating frequency of impact printers. Hendriks [10] suggested that passive damping methods be improved, probably requiring a breakthrough in materials, and/or that driving current waveform ought to be respond to the phase of the hammer motion and the pattern to be printed. Wen [17] claimed that the settling time in impact printers was reduced while printer speed and reliability were increased by using a separate return solenoid magnet to accelerate the motion of the hammer to its rest position thus significantly reducing the damping time. In dot matrix impact printers of stored energy type, the energy to propel the armature is completely gained from the prestressed spring. Good print

quality can be achieved if a sufficient energy is stored in the driving spring in order to gain a sufficient printing force [18-19]. For the purpose of attaining a sufficient print force, the print hammer is generally improved by increasing its spring coefficient and displacement from spring rest position. Furthermore, the permanent magnetic field could be increased for better stability [20-21]. Chiu et al. [22] found that by a certain arrangement of auxiliary magnetic poles of dual magnet loops and the center of rotation of the armature [8] the capability of high speed printing and good stability were achieved. Generally, the stored energy type impact printer head is an application of magnetic flux loop. A general structure comprises an iron core, a nonmagnetic coil, spring, armature, wire, yolk, ring, permanent magnet and core base. Chiu et al. [22] claimed that by using the added magnetic pole of dual magnetic design, the offset energy produced by conventional magnetic flux can be induced and shifted to another pole which produces a force to attract the armature. Carson and Harris [15] devised a control system in which damping pulses were applied to the armature after its return to the backstop from the paper. This minimizes bounce of the armature against the backstop. The energy content of the driving pulse was varied in proportion to the amount of overlap between the driving pulse and the proceeding damping pulse. The above control strategies require expensive damping materials and/or additional sensors and digital signal processing.

From the above we observe that most of papers, except Hendriks' [10], did not consider the effects due to impact at the backstop. Also, the general dynamic response of impact printers was not

investigated in those works. In this dissertation a piecewise linear model is used to study the dynamics of the print hammer and a simple impact rule employing a coefficient of restitution is adopted to characterize the bounce behavior at the backstop. Similar impacting systems can be found in [23-35]. Also, a simple low cost, highly efficient, open-loop control strategy to increase the operating speed and the dynamic stability of the print hammer is introduced. Printer performance criteria are also presented and shown to be useful in the evaluation of general control strategies.

Previous work on impacting systems is vast and includes that of Masri [23] who examined the existence and stability of periodic symmetric two impacts per cycle motions for the impact damper. Senator [24] studied an impacting system with constant restoring force, harmonic excitation, and energy dissipation upon impact which modeled a vibratory plow. In Senator [24] necessary conditions were found for the existence of periodic motions with one impact per motion cycle and their stability was investigated by using a procedure similar to that in [23]. This procedure involves examination of the behavior of small perturbations near the periodic solution. Holmes [25] investigated the dynamics of a mass bouncing on a sinusoidally vibrating table using a discrete-time dynamics approach. In his paper harmonic, subharmonic and chaotic motions were found and analyzed by employing bifurcation theory and topological methods. Shaw and Holmes [26] considered a periodically forced single degree-of-freedom piecewise linear system with a single change in restoring force slope. In that paper harmonic, subharmonic, and chaotic motions were found to exist. Similar works were extended to impacting systems with large

dissipation due to impact which may model mechanical systems having amplitude constraints with highly inelastic materials (Shaw and Holmes [27]), with rigid two-sided amplitude constraints which may model linkages, gears, and fasteners with looseness or play (Shaw [28-29]), and with dry friction which may model the mechanical system in which components are in contact with one another and are free to slide relative each other (Shaw [30]). Heiman et al. [31] studied the dynamics of an inclined impact pair which modeled an impact damper. The stability of the periodic motion of two impacts per forcing cycle was investigated by using a Poincare map. Period doubling bifurcations and saddle node bifurcations were analyzed in that paper. In Bapt and Sankar [32] a simulation method was employed to study the characteristics of an impact damper at various parameters such as mass ratio, coefficient of restitution and gap size. Whitson [33-34] investigated the harmonically excited and preloaded vibro-impacting system. Local and global dynamics of the preloaded system were thoroughly studied. Domains of attraction and stability regions for various steady state motions were explored by using Poincare maps and bifurcation theory together with simulations. In Whitson [35] the singularity structure in vibro-impact dynamics of an undamped linear oscillator were studied. The singularity structure is related to the zero velocity impacts, i.e., degenerate impacts. Trapping and chatter phenomena and the associated chaos were discussed in that paper. The above references [23-35] also contain many other references related to systems with clearances, etc.

The above mentioned references all consider response of impacting systems to purely harmonic, periodic input. In this dissertation a

piecewise linear impacting system with nonharmonic periodic excitation and nonperiodic inputs, which more realistically models actual printer inputs, is used to study the dynamics of the stored energy type impact printer.

1.3 Scope of the Investigation

In this thesis the dynamics of a model of an impact print hammer of the stored energy type is studied and a control method for the improvement of printer performance is proposed. The methods from dynamical systems and bifurcation theories are employed to study the piecewise linear model. The scope of the investigation of this dissertation are as follows:

- 1) To determine parameters such that the model used in this dissertation mimicks Hendriks' model, which is known to be an accurate model for a particular type of stored energy impact print hammer [10].
- 2) To determine the periodic motions with n backstop impacts per forcing cycles (the forcing is assumed to be periodic). For nonlinear dynamic systems, there may not exist a stable periodic motion for such an input. Using the solutions of piecewise linear equations of motion and the conditions for the existence of a periodic motion, we can obtain the conditions of the periodic solutions and solve these numerically. The response of these periodic motions for a range of forcing periods are to be considered.
- 3) To determine the stability of the periodic motion using the concept of a Poincare map and a Poincare section. Two types of Poincare

sections are employed. An unstable motion may cause print force variations which affect print quality.

4) To determine the bifurcation conditions, i.e., determine where stability is lost and how different parameters affect stability. Bifurcation curves for different parameters are generated and examined.

5) To determine the influence of various parameters on the performance of impact printers. We consider the possibility of increasing operating speed and/or extending stability ranges in this case.

6) To compare our results with those of Hendriks'. Can we predict the same qualitative behavior as that of the more complicated model due to Hendriks ?

7) To determine where chaotic motions and strange attractors exist in the parameter space using Poincare maps and digital simulations in conjunction with the stability analysis.

8) To study and characterize the chaotic dynamics of the system by use of digital simulations to determine when the stable and unstable manifolds of certain saddle-type periodic motions intersect transversally, which implies that there exists a Smale horseshoe for the dynamics (it is a complicated invariant set containing infinite families of periodic and nonperiodic motions). Also to prove there exists an attracting set which contains these horseshoes, resulting in bounded, irregular dynamics.

9) To obtain Lyapunov exponents which measure the average exponential rates of divergence or convergence of nearby orbits in phase space for chaotic motions.

10) To increase the operating speed of impact printers. The armature motion is extremely sensitive to the timing of the refiring. This sensitivity can cause instabilities of motions and is detrimental to print quality. Thus current impact printers are operated at low frequencies to allow enough time for settle-out without affecting the subsequent firing cycle. It has been found that by increasing the pre-load during the settle-out phase, one can achieve rapid settle-out and hence increase the operating speed. An open-loop control strategy which consists of applying an inverted pulse, of opposite sense to the driving pulse, to the coil, thus aiding the force of permanent magnet during the settle-out phase, is proposed. This inverted pulse increases the net magnetic field which holds the armature against the backstop causing a decrease in the settle-out time. Thus settle-out occurs more quickly and all phase-space trajectories are quickly mapped into a region near the rest position. This provides acceptable conditions for the refiring and results in acceptable print quality.

11) Printer performance criteria are to be established.

Actual printers are subjected to irregularly timed pulses, i.e., "firing combinations," which depend on the distance between dots which form the desired characters. Printer performance criteria are to be established based on the requirement that acceptable print quality be achieved for a class of arbitrary firing combinations with some minimum period between pulses. This minimum period is typically the lowest period which provides acceptable steady state, i.e., periodic, operation. This must also hold for all physically possible initial conditions which may be provided at the time of refiring. This condition is necessary since the print hammer must be fired before

settle-out is complete if the printer is to run at an increased operating speed.

Items 1-8) deal with strictly periodic input, the related results will characterize the dynamic response of the print hammer model. Items 9-10) deal with more realistic, nonperiodic inputs. The control method will be applied to the system and tested with both types of input.

The main contribution of this dissertation are:

- 1) The methods of dynamical systems and bifurcation theory are applied with success to a piecewise linear model of an impact print hammer with nonharmonic periodic and nonperiodic excitation.
- 2) A simple method of increasing the operating speed of impact printers is proposed and tested by simulation.
- 3) New printer performance criteria and means of verification of these are established using ideas from dynamical system theory.

1.4 Dissertation Arrangement

This dissertation is arranged as follows. In Chapter 2 a mathematical piecewise linear model which characterizes the impact printers of the stored energy type is introduced. It also provides a review of Poincare maps and bifurcation theory and their utility in studying periodically forced oscillators. In Chapter 3 we study the dynamic response of our impact printer model by considering periodic input. The existence and the stability of periodic motions are

discussed. Also, we present simulation results and make some general observations regarding the system response for various parameter conditions. The chaotic dynamics of the system are characterized by finding the intersection of the stable and unstable manifolds, strange attractors, and Lyapunov exponents. In Chapter 4 an open-loop control strategy is proposed and printer performance criteria are established and verified by using a form of a Poincare map. Limitations on printer speed are demonstrated and we indicate how the control method is able to increase the printer speed. In Chapter 5 we close the dissertation with some conclusions and directions for future work.

CHAPTER II

MODEL AND METHODS OF ANALYSIS

2.1 Mathematical Model

This dissertation discusses the dynamic behavior of a simplified model for an impact print hammer. We consider only dot matrix printers of the stored energy type as shown in Figure 1. A mass, called the armature, is held by a permanent magnet until a dot on the paper is desired. When energized with a current of appropriate sense and magnitude, a coil will produce a magnetic field which opposes the field of the permanent magnet and will release the deflected spring. This spring propels the print wire, which is attached to the armature, to strike the ribbon and paper. Upon returning from the ribbon and paper the armature, due to the permanent magnet force, hits the backstop and rebounds against the backstop during "settle-out" until it is energized again. It should be noted that the net force which holds the armature is very small. Thus energizing a small amount of current will release the armature.

Referring to Hendriks' model for print hammer [10], we propose the model shown in Figure 2. A mass m is attached to a linear pre-loaded spring with negative stiffness k_1 which characterizes the net effect of the permanent magnet and the prestressed spring(see Fig. 2 in [10]), and to a linear dashpot with damping constant c_1 which models energy dissipation in the system. The mass is held against the

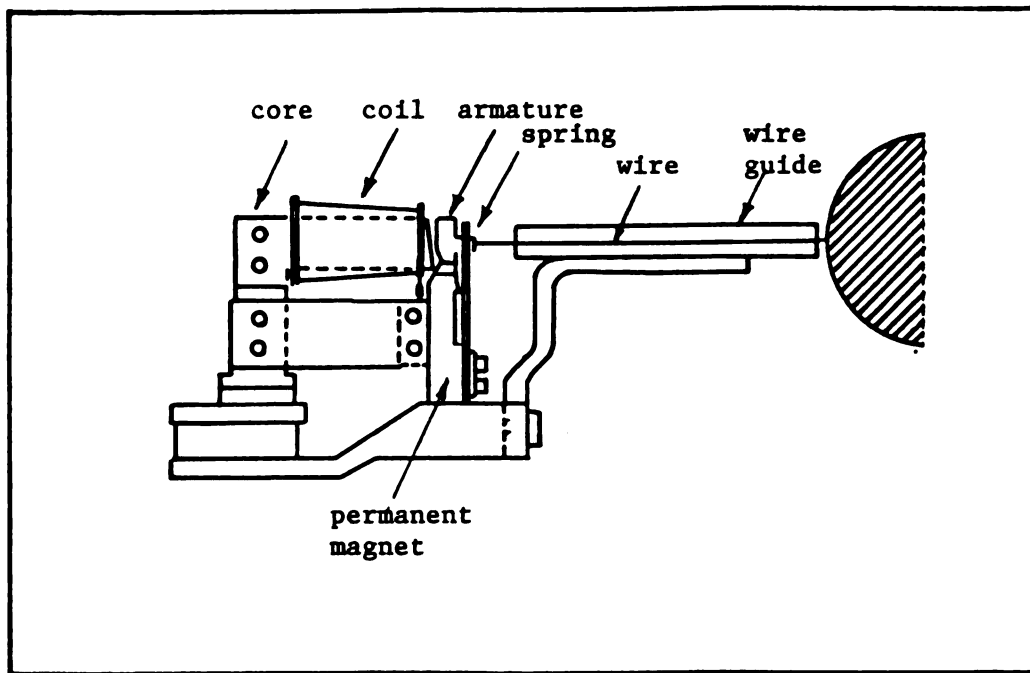


Figure 1. Impact printer of the stored energy type (from [10] with permission from the Editor, IBM Journal of Research and Development)
 "Copyright 1983 by International Business Machines Corporation"

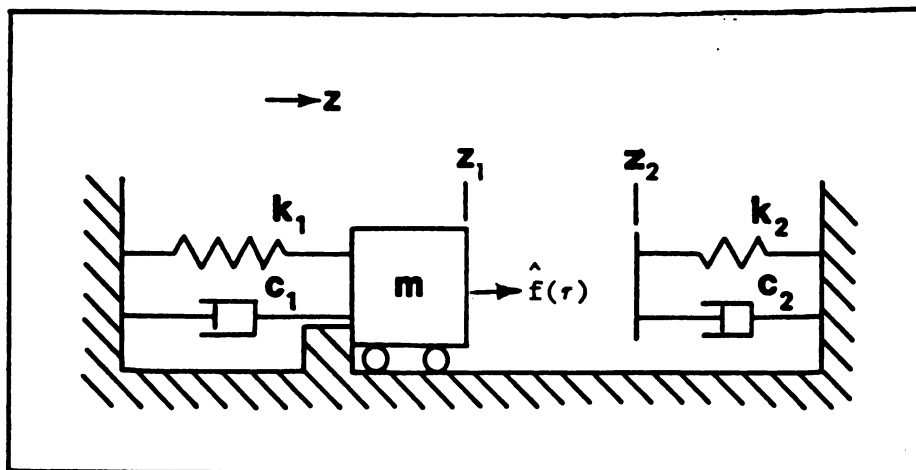


Figure 2. A model of the simplified dynamical system

backstop by the pre-loaded spring. When excited by a periodic half sine-wave pulse, the mass leaves the backstop and strikes the linear spring k_2 and the linear dashpot c_2 which represent the net effect of the ribbon and paper. After returning from the paper, the mass hits the backstop and rebounds of successively smaller amplitude occur until the mass is excited by a next pulse. A coefficient of restitution, r , which depends on the impact velocity and the backstop material is adopted to characterize the rebound phenomenon.

The equations of motion can be written as follows:

$$mz'' + c_1 z' - k_1(z - z_0) = \hat{f}(\tau) \quad ; \quad z_1 < z < z_2 \quad (2.1.1)$$

$$mz'' + (c_1 + c_2)z' - k_1(z - z_0) + k_2(z - z_2) = \hat{f}(\tau) \quad ; \quad z \geq z_2 \quad (2.1.2)$$

where $(\)'$ is defined as a time derivative $d/d\tau$, $k_1 z_0$ represents the force due to the pre-load in the spring, z_2 is the position of the ribbon and paper, and

$$\hat{f}(\tau) = \begin{cases} F \sin(\hat{w}\tau) & \text{while a pulse is acting} \\ 0 & \text{otherwise} \end{cases} \quad (2.1.3)$$

and $\hat{w} = \pi/\hat{D}$, \hat{D} is the duration of a sine pulse and F is the forcing amplitude. At $z = z_1$ impact occurs at the backstop and a simple impact rule is applied:

$$z'(\tau^+) = -rz'(\tau^-) \quad \text{with} \quad (\tau^+ - \tau^-) \rightarrow 0 \quad (2.1.4)$$

where r is the velocity dependent coefficient of restitution:

$$r = \delta + \hat{\alpha} z'(\tau^-) \quad \text{for} \quad z'(\tau^-) < v_0 \quad (2.1.5)$$

$$r = b \quad \text{for} \quad z'(\tau^-) < v_0 \quad (2.1.6)$$

and $\delta, \hat{\alpha}$ are constant factors which depend on the backstop material [36]. The coefficient of restitution r is a decreasing function of increasing impact velocity $z'(\tau^-)$. However, it cannot, for obvious physical reasons, be a negative value, thus equation (2.1.5) is only applicable for a limited range of impact velocities. For higher velocities $z'(\tau^-)$, an adjusted equation, (2.1.6), of constant r will be used to characterize the bounce phenomenon at the backstop.

Simplified equations can be obtained through rescaling by letting

$t = \sqrt{\frac{k_1}{m}} \tau$ and $x = \frac{z}{c}$ where c is a constant factor which rescales the amplitude z . In the actual system, the travel distance of a print hammer is only around 0.1524 mm (0.0006 in) [10]. Amplification of the amplitude of the mass displacement will be used for convenience in simulations and other computer analysis. In this dissertation we set $c=0.01$ in to make the distance between the backstop and the paper be

equal to 0.6 in dimensionless units. The rescaled equations are written as:

$$\ddot{x} + 2\alpha_1 \dot{x} - x + F_0 = f(t) \quad ; \quad x_{01} < x < x_{02} \quad (2.1.7)$$

$$\ddot{x} + 2\alpha_2 \dot{x} + k^2 x - (1.0 + k^2) x_{02} + F_0 = f(t) \quad ; \quad x \geq x_{02} \quad (2.1.8)$$

$$\dot{x}(t^+) = -r \dot{x}(t^-) \quad ; \quad x = x_{01} \quad (2.1.9)$$

$$r = \delta + \alpha \dot{x}(t^-) \quad \text{for } \dot{x}(t^-) < v_1 \quad (2.1.10)$$

$$r = b \quad \text{for } \dot{x}(t^-) \geq v_1^* \quad (2.1.11)$$

where $(\dot{}) = \frac{d}{dt}$, $\alpha_1 = \frac{c_1}{2\sqrt{k_1 m}}$, $\alpha_2 = \frac{c_1 + c_2}{2\sqrt{k_1 m}}$, $F_0 = \frac{z_0}{c}$,

$$k = \sqrt{\frac{k_2 - k_1}{k_1}}, \quad x_{01} = \frac{z_1}{c}, \quad x_{02} = \frac{z_2}{c}, \quad \alpha = \hat{\alpha} c \sqrt{\frac{k_1}{m}},$$

$$v_1 = v_0 \hat{\alpha} c \sqrt{\frac{k_1}{m}}, \quad \text{and}$$

$$f(t) = \begin{cases} \beta \sin(\omega t) & \text{while a pulse is acting} \\ 0 & \text{otherwise} \end{cases} \quad (2.1.12)$$

* The value of v_1 should be such that $\dot{x}_1(t^+) < \dot{x}_2(t^+)$ if $|\dot{x}_1(t^-)| < |\dot{x}_2(t^-)|$ for most backstop materials. The v_1 value used in this thesis allows this condition to be violated at impact velocities above 0.75 (it does not allow $\dot{x}(t^+) < 0$). This behavior is not typical of most materials.

with $\beta = \frac{F}{k_1 c}$, $\omega = \frac{\pi}{D}$, and $D = \hat{D} \sqrt{\frac{k_1}{m}}$.

Local solutions of the equations (2.1.7)-(2.1.11) can be obtained explicitly. Such solutions can be repeatedly matched at $x = x_{01}$ and $x = x_{02}$ to obtain a global solution of the system. However, piecing together these known equations is not explicitly possible since the times of flight in each region and the time when the pulse is acting cannot be found in closed form.

In order to predict the same qualitative behavior of the impact print hammer as Hendriks [10], we set the values of the parameters (α_1 , α_2 , k , δ , α , F_0 , β , D , b) by referring to the diagram of the net force due to the magnetic field and the linear spring versus distance and the diagram of the force-displacement in [10]. Then by trial and error parameters were adjusted to match the phase portrait of a single pulse motion started from rest. The results from our model are shown in the plot of the phase portrait in Figure 3(a), the plot of the phase portrait in Figure 3(b) reproduces the response from Hendriks' model [10].

Figure 4 shows a plot of the net restoring force versus displacement for our model. Figure 5 depicts a forcing function which consists of periodic sine pulses. Figures 6(a) and (b) shows plots of phase portraits (velocity versus displacement) of the steady state system response to such an input with a single impact (at the

backstop) per forcing cycle and two impacts per forcing cycle respectively.

The plots of the phase portrait in Figures 3(a) and 6 are generated by digital simulations of equation (2.1.7)-(2.1.11). The simulations are easily be performed by piecing together the solutions from each piecewise linear equation and solving the boundary conditions, i.e. the crossing time and crossing velocity at $x = x_{01}$ and $x = x_{02}$ by using Newton-Raphson method.

2.2 Methods of Analysis

From the equations of motion (2.1.7)-(2.1.11), we see that a three dimensional extended phase space with co-ordinates (x, y, \dot{x}, t) can specify the state of this one degree-of-freedom periodically forced system. By taking the time t as a parameter and projecting a trajectory to the two dimensional plane (x, y) , we obtain a plot commonly referred to as the phase plane, or phase portrait, as shown in Figures 3 and 6. The motion in Figure 6(a) takes point A at the backstop, $x=0.2$, through points 1,2,3,4 and 5, and back to point B at the backstop. We see that the time and velocity at the starting point A will uniquely determine the time and velocity at the next similar encounter, point B at the backstop. It should be noted that the orbit is a periodic orbit if the point A and the point B coincide at identical forcing phases. To determine B we may, in principle, write:

$$t_B = f(t_A, y_A) \quad (2.2.1a)$$

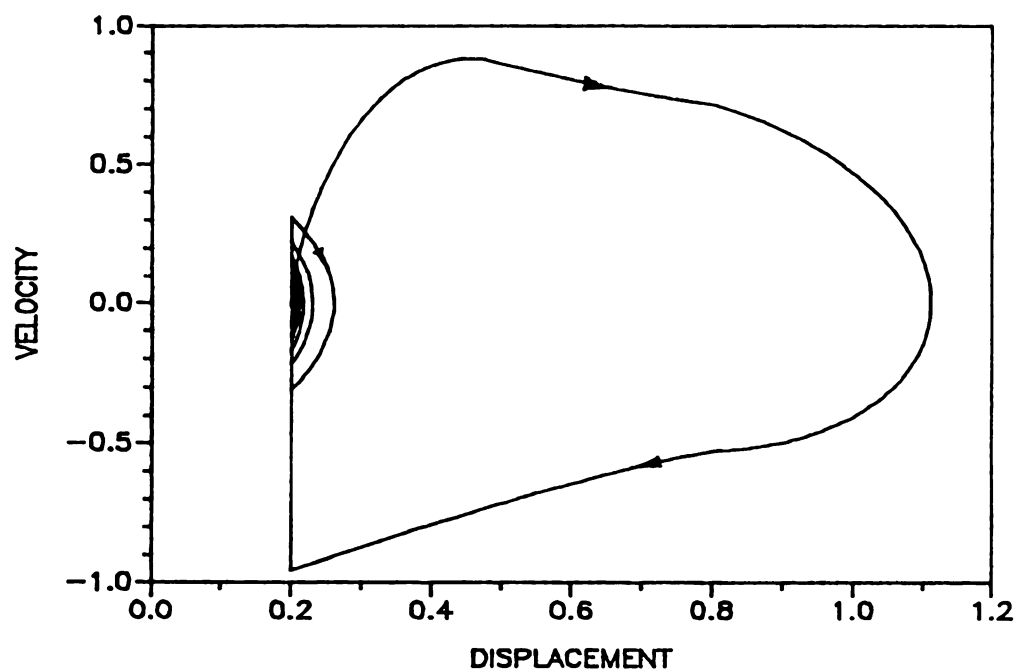


Figure 3(a). The phase portrait with single sine pulse excitation, $\beta=3.2$, $\alpha_1=0.005$, $\alpha_2=0.2$, $k=1.56$, $F_0=1.0345$, $D=0.66$, $\delta=0.9$, $\alpha=0.6$, $x_{01}=0.2$, $x_{02}=0.8$, $b=0.15$.

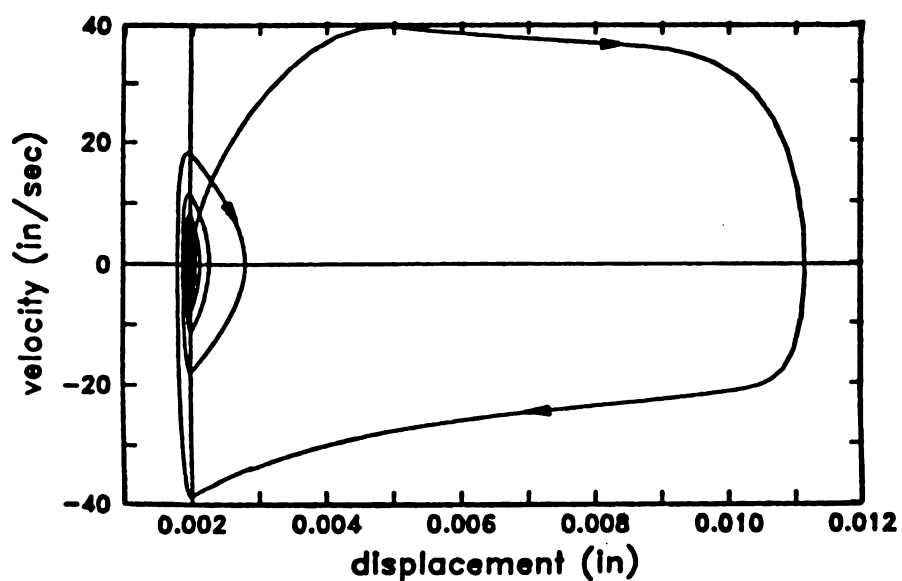


Figure 3(b). The phase portrait from Hendriks' model (from [10] with permission of the Editor, IBM Journal of Research and Development)
 "Copyright 1983 by International Business Machines Corporation"

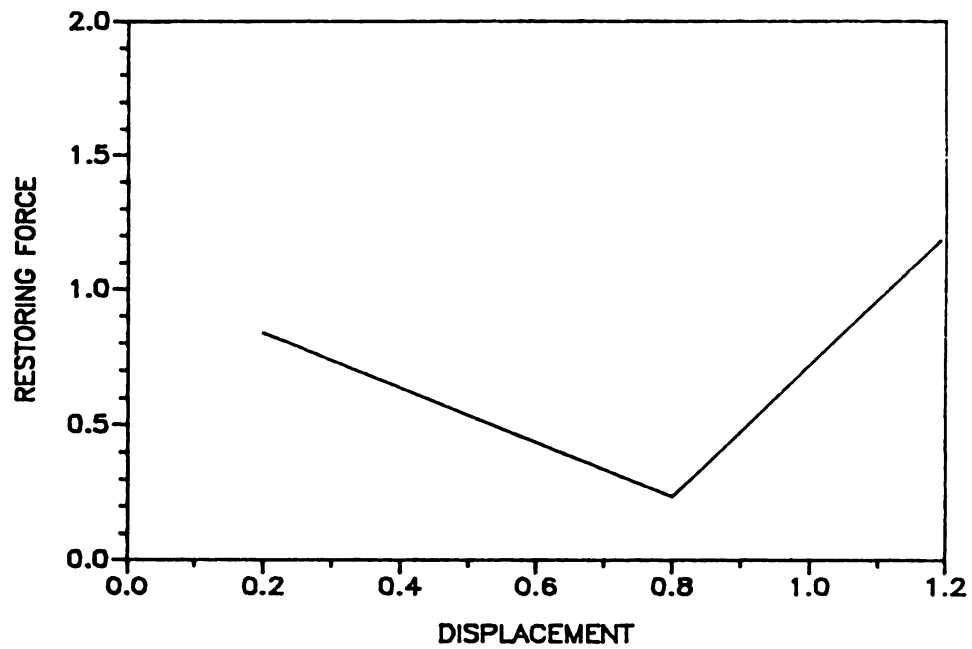


Figure 4. The net restoring force versus time.

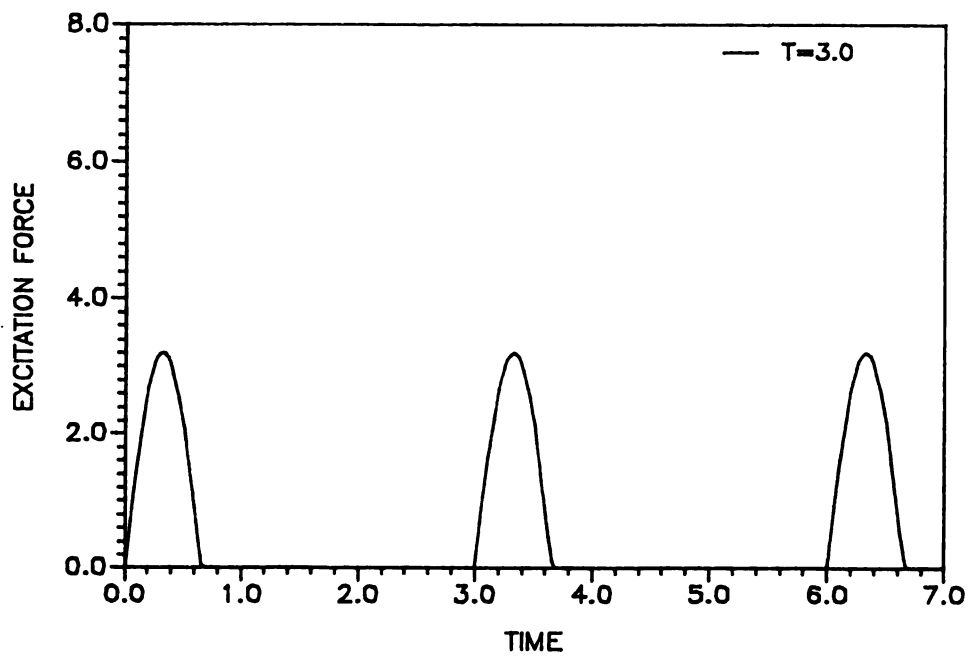


Figure 5. The periodic excitation force versus time

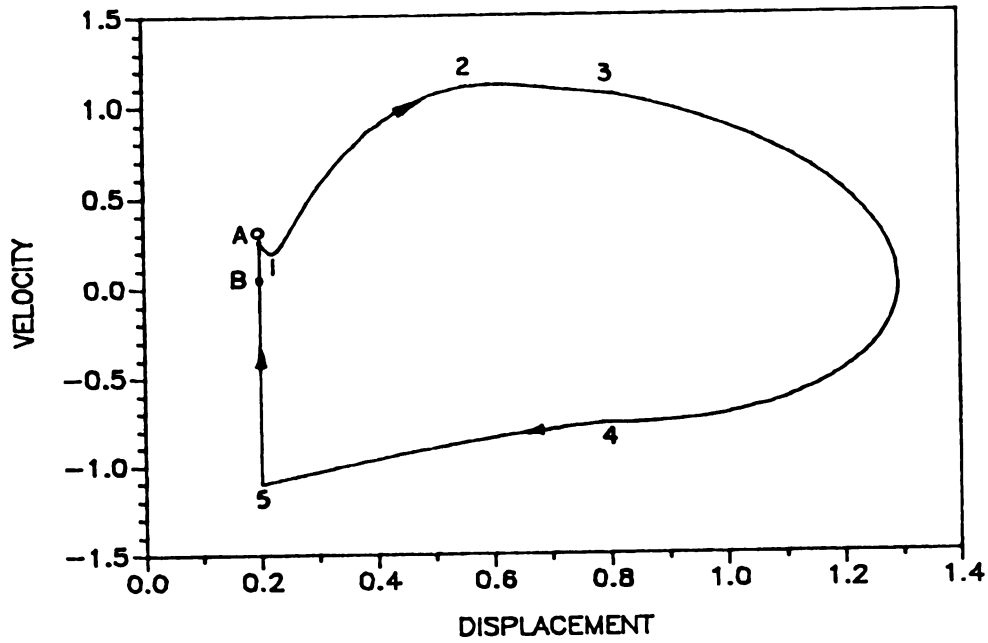


Figure 6(a). Phase portrait with single impact per forcing cycle.

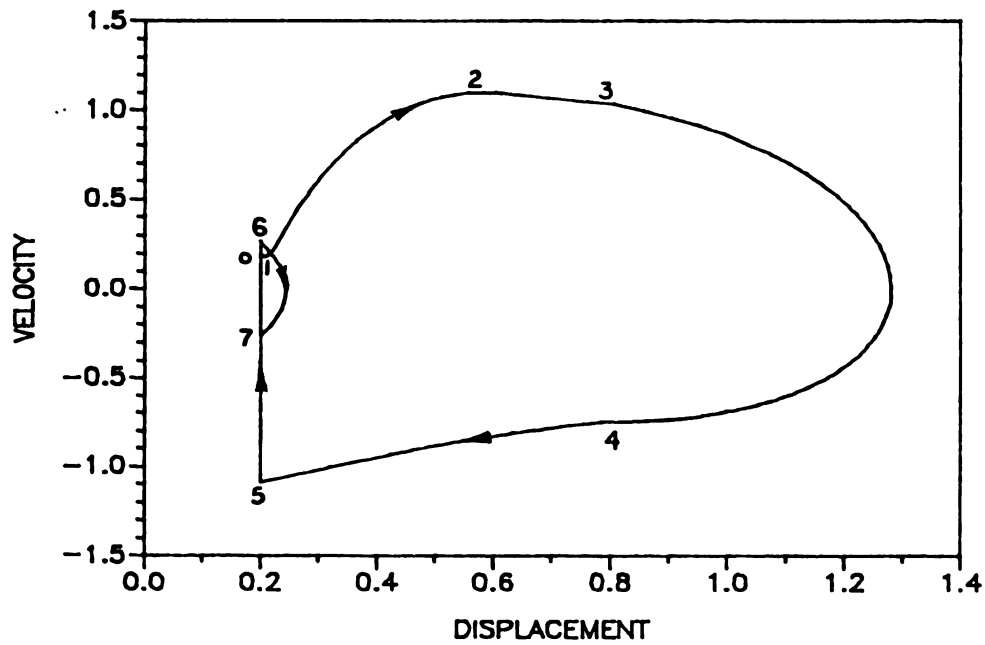


Figure 6(b). Phase portrait with two impacts per forcing cycle

$$y_B = g(t_A, y_A). \quad (2.2.1b)$$

In this way simple recursion relations, referred to as maps, are used to study the behavior of the system.

To generalize this idea, consider a function P which maps a point on a chosen two-dimensional surface in (x, y, t) space, back to the same surface under the governing equations of motion. Such a function is called the Poincare map. The surface, or cross-section, is called the Poincare section Σ and must be transverse to solution trajectories. We then write $P: \Sigma \rightarrow \Sigma$ and P represents a specified means of discretizing the dynamics of the system.

In periodically forced systems, a Poincare map is often used which stroboscopically samples (x, \dot{x}) points at time values $t = t_0 + nT$, where $n = 1, 2, \dots$ and T is the forcing period. The Poincare section is then defined as

$$\Sigma^{t_0} \subset \mathbb{R}^2 = \{(x, y, t) \mid t = t_0 \bmod(T)\} \quad (2.2.2)$$

and the Poincare map is defined as

$$P^{t_0}: \Sigma^{t_0} \rightarrow \Sigma^{t_0} \quad \text{or} \quad (x_{i+1}, y_{i+1}) = P^{t_0}(x_i, y_i). \quad (2.2.3)$$

Here t_0 simply represents the particular phase of the periodic forcing at which the pulse is applied.

Referring to equations (2.1.7)-(2.1.11), we see that our model has a piecewise linear structure. Nonlinearities occur at $x = x_{01}$ and $x = x_{02}$ due to the change in dissipation and restoring force coefficients. Similar to the methods described in [25-30], we can employ another type of Poincare map to study the dynamics of this system. It is often convenient to choose Σ at a place where a discontinuity in stiffness occurs. In our system the Poincare section can be defined as those points in the phase space which correspond to states at which the mass hits the backstop, i.e.,

$$\Sigma_1 \subset \mathbb{R}^+ \times S^1 = \{(x, y, \phi) \in \mathbb{R}^2 \times S^1 \mid x = x_{01}, y > 0\} \quad (2.2.4)$$

where $\phi = t(\text{mod } T)$ is the phase of the forcing.

The associated mapping P_1 is equivalent to functions f and g in equation (2.2.1). This section and map exploit the piecewise linear nature of the system. We will use both Poincare sections, and their associated maps, in the analysis as is convenient.

By using a Poincare map we can reduce the study of the system from that of a three dimensional continuous phase space (x, y, t) to an iterated mapping, i.e., a discrete time system, with two variables. A fixed point of a map is represented as follows: $P(\bar{\zeta}) = \bar{\zeta}$ with $\zeta \in \Sigma$.

A periodic point is a point $\bar{\zeta}$ such that $P^j(\bar{\zeta}) = \bar{\zeta}$. (Note that $\bar{\zeta}$ is a fixed point of the j th iterate of P , P^j). These types of points represent periodic behavior of the system. The stability type of a

fixed point of the Poincare map corresponds to the stability type of the corresponding periodic motion.

The stability of a nonlinear system can be studied by using the Lyapunov direct method [36-38]. The method relies on finding a positive definite function called the Lyapunov function which decreases along the solution curve of the differential equations. In fact, in many physical problem the total energy stored within the system is the logical choice for a Lyapunov function. The idea of this method is a generalization of the concept of energy and its power and usefulness lies in the fact that the stability is explored by investigating the differential equations itself and not finding the solutions of the differential equations. However, in general it is difficult to find a Lyapunov function. This method can be applied to autonomous systems and nonautonomous systems with the existence of equilibrium points. There are no equilibrium points for nonautonomous system such as oscillators with external forcing. In this dissertation due to the piecewise nature and large external forcing in the system, the Lyapunov direct method is not applicable. Thus linearization method is employed to determine local stability of periodic motions. This method consists of linearizing the given system in the neighborhood of a fixed point of the Poincare map or a equilibrium point of the flow and determining the behavior of the nearby solution trajectories by studying the resulting linear system. The periodic orbits of interest in the present case pierce one of the sections Σ in a single point and thus represent a fixed point for the map P . Local stability can be investigated by linearizing the map P about the periodic point

$$(\xi_{i+1}, \eta_{i+1}) = DP(\xi_i, \eta_i) \quad (2.2.5)$$

where (ξ, η) is a small perturbation about the periodic point and DP is the Jacobian of P evaluated at the periodic point.

The Hartman-Grobman theorem states that if $DP(\tilde{\zeta})$ has no eigenvalues of unit modulus, the eigenvalues of $DP(\tilde{\zeta})$ determine the local stability of the associated motion [39].

Hartman-Grobman theorem (for maps): Let $P: \mathbb{R}^n \rightarrow \mathbb{R}^n$ be a $(C)^1$ diffeomorphism with a hyperbolic fixed point $\tilde{\zeta}$. Then there exist a homeomorphism h defined on some neighbor U on $\tilde{\zeta}$ such that $h(P(\nu)) = DP(\tilde{\zeta})h(\nu)$ for all $\nu \in U$. The proof of the theorem can be found in [40-41]. P is a diffeomorphism if P is a smooth map with a smooth inverse. A fixed point $\tilde{\zeta}$ is called a hyperbolic if the derivative DP has no eigenvalue of unit modulus. Then the asymptotic behavior of solutions near the fixed point are determined by the linearization. If any one of the eigenvalues has the unit modulus, then the stability cannot be determined by linearization. In our case the mapping P cannot be written down explicitly. In fact, P is not always well defined since some points in Poincare section Σ are mapped onto the line $y=0$. A degenerate impact occurs and leads to discontinuity in the mapping (see Shaw and Holmes [26-27] and Whitson [35] for details). In such case the map P is not smooth and Hartman-Grobman theorem is not directly applicable. The linearized map DP can be computed directly by using implicit differentiation.

For a two dimensional map, both eigenvalues of DP evaluated at the fixed point lie in the complex plane. If both eigenvalues lie inside the unit circle in the complex plane, i.e., when $|\lambda_i| < 1$, $i=1$ and 2 , the motion is locally asymptotically stable and if either eigenvalue lies outside the unit circle the motion is unstable. Detailed discussion about different locations of the eigenvalues and the stability of the associated motion follows. If $\lambda_1 < 1$, $\lambda_2 < 1$ and $\lambda_{1,2}$ are real, the corresponding fixed point is a stable node and the local steady state motion is periodic. In the phase space there exists an associated stable limit cycle. If $\lambda_1 < 1$, $\lambda_2 > 1$ and $\lambda_{1,2}$ are real, the fixed point is a saddle and the associated motion is locally unstable. The corresponding unstable period orbit in phase space will be generally unobservable. If $\lambda_1 > 1$, $\lambda_2 > 1$ and $\lambda_{1,2}$ are real, the fixed point is an unstable node and the associated motion is locally unstable. If λ_1, λ_2 are complex, they must exist as a complex conjugate pair and the local map has a rotational behavior associated with it. The eigenvalues can be written as $\lambda_{1,2} = \alpha + \beta j = |\lambda| e^{\pm \theta j}$,

$$|\lambda| = \sqrt{\alpha^2 + \beta^2}, \quad \theta = \tan^{-1}\left(\frac{\beta}{\alpha}\right) \text{ (see Shaw [30] for details). The}$$

corresponding rotation number is given by $\rho = \frac{\theta}{2\pi}$. If $|\lambda| < 1$, the fixed point is a stable focus and the associated transient behavior near the steady state periodic motion is a decaying oscillatory behavior superimposed on the stable periodic motion. This leads to a decaying beating-type motion. The inverse of the rotation number is

approximately equal to the number of cycles in one period of the envelope. If $|\lambda| > 1$, the fixed point is an unstable focus and the associated motion is locally unstable. If $|\lambda| = 1$, the stability type is very complicated and cannot be determined by linearization. Center manifold technique need to be used to study those nonlinear phenomena. No $|\lambda| = 1$, λ complex, bifurcations were found to occur for the printer model.

"Local" in the above means that the motion behavior can only be predicted near the fixed point. In nonlinear systems there may exist many stable limit sets and the steady state behavior is dependent on initial conditions.

2.3 Bifurcation

As system parameters are varied, eigenvalues may pass through the unit circle, at which point a bifurcation occurs and the dynamical response changes, i.e., the qualitative behavior of the system changes. The changes are called bifurcations and the corresponding parameter values are called bifurcation values. It should be noted that when a discontinuity in map exists and a fixed point crosses it, the qualitative behavior of the system will also change (as will be seen in this dissertation). However, this change is not a standard bifurcation.

Bifurcations can be described as local or global. If a particular bifurcation is related to behavior near a nonhyperbolic fixed point (bifurcation point), the bifurcation is local in nature.

Others, which involve changes in the global structure of the phase space are global bifurcations. For studying the local behavior near the bifurcation point, center manifold techniques can be employed. A center manifold W^c is a invariant manifold tangent to the center eigenspace E^c , i.e., the eigenspace associate with nonhyperbolic eigenvalues. One can reduce the map (or flow) to the center manifold and investigation of the map (or flow) on W^c will determine the stability types and changes that occur at the bifurcation point. See Carr [42].

Eigenvalues with -1 are associated with flip bifurcations, which are also referred to as period doubling bifurcations. This bifurcation is a very common type of bifurcation in nonlinear systems. The period doubling bifurcation involves the birth of a new periodic motion with period double that of the original period. There are two types of period doubling bifurcations. Figure 7(a) shows a supercritical period doubling bifurcation in which a stable periodic orbit of period T loses its stability and becomes unstable with the appearance of a stable periodic orbit of period $2T$. Figure 7(b) shows a subcritical period doubling in which an unstable periodic orbit of period $2T$ merges with the stable periodic orbit of period T and an unstable periodic orbit of period T remains. In a nonlinear system once one of the eigenvalues passes through -1 as system parameters are varied, a period doubling sequence will typically appear, i.e., a motion of period T goes through periods $T 2^n$, $n=1,2,3,\dots$ (unless a discontinuity is encountered) and eventually results in an infinitely long periodic motion, or chaotic motion. The cascades of period

doubling are typical behavior for nonlinear systems. See Feigenbaum [43] for results which indicate the universal nature of these period doubling sequences. The stability type of a period doubling bifurcation (subcritical or supercritical) can be determined by using the center manifold technique. This procedure reduces the map being considered to a local one-dimensional map as described in [26] and yields the following generic form:

$$u_{n+1} = - (1 + \mu) u_n + a u_n^2 + b u_n^3 \quad (2.4.1)$$

for the behavior on W^C for μ and u nearly zero. μ is the bifurcation parameter and u is the co-ordinate on a local center manifold.

The origin $\tilde{u} = 0$ is always a fixed point and is stable for parameter $\mu < 0$. Using the second iterate of this map it can be shown that $b+a^2 > 0$ (< 0) corresponds to a super (sub)-critical bifurcation.

As system parameters are varied and an eigenvalue passes through $+1$, there are three possible bifurcations: the saddle-node bifurcation, the pitchfork bifurcation and the transcritical bifurcation. The center manifold method yields a one-dimensional map which determines the local dynamics at the bifurcation point. Only saddle node bifurcations are considered here. See Guckenheimer and Holmes [39] for details concerning the other types. At a saddle-node bifurcation a pair of orbits, one a stable node and the other a saddle, coalesce and annihilate one another as shown in Figure 8.

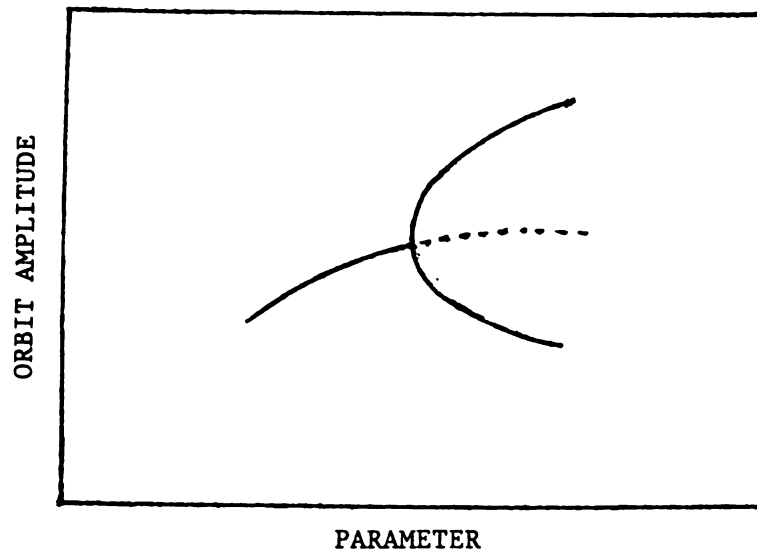


Figure 7(a). A supercritical flip bifurcation (the bifurcated motion alternates between branches).

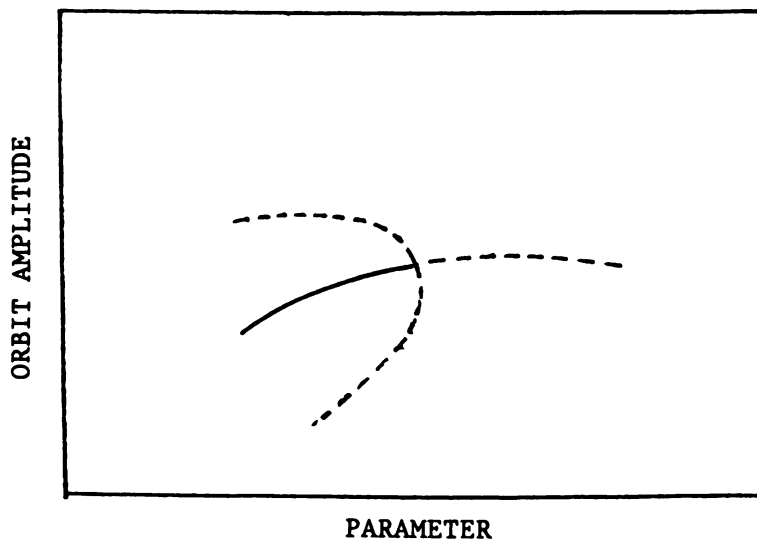


Figure 7(b). A subcritical flip bifurcation.

In the case that eigenvalues are complex with $|\lambda| = 1$, a Hopf bifurcation occurs. If the determinant of $DP(\bar{\xi})$ is less than 1, no Hopf bifurcations can occur because eigenvalues cannot pass through the unit circle as a complex conjugate pair since $\lambda_1 \lambda_2 < 1$. No Hopf bifurcations were found to occur in our model since $\lambda_1 \lambda_2 < 1$ was always satisfied. In fact, only period doubling bifurcations were found to occur for the printer model dynamics.

Global bifurcations occur in the model but are not considered here. They result in the chaotic dynamics observed in simulations.

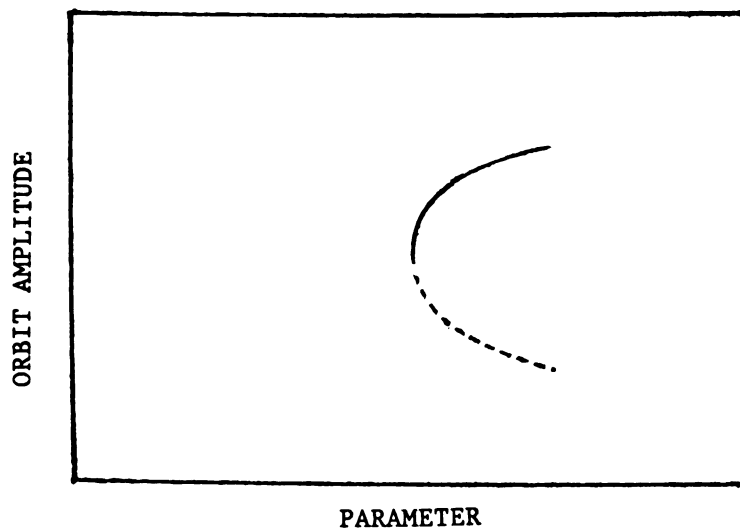


Figure 8. a saddle-node bifurcation

CHAPTER III

THE DYNAMIC RESPONSE : PERIODIC INPUT

3.1 Existence of Periodic Motions

In this section we exploit the piecewise linear nature of our model in order to obtain explicit conditions for the existence of periodic motions. The analysis involves the piecing together of several trajectory pieces in the various linear regions in such a manner that the motion is repetitive, i.e., periodic.

Referring to the phase portrait shown in Figure 6, the solutions to equation (2.1.7) based at (x_0, y_0, t_0) are

$$\begin{aligned} x(t; y_0, t_0) = & e^{-\alpha_1(t-t_0)} [A_0 \cosh(\Omega_1(t-t_0)) + B_0 \sinh(\Omega_1(t-t_0))] \\ & + F_0 \end{aligned} \quad (3.1.1)$$

for $t_0 \leq t < t_1$ where t_1 is the time when a sine pulse starts to apply. For the next part of the motion

$$x(t; y_0, t_0) = e^{-\alpha_1(t-t_0)} [A_0 \cosh(\Omega_1(t-t_0)) + B_0 \sinh(\Omega_1(t-t_0))]$$

$$\begin{aligned}
& + F_0 + (\beta/2\Omega_1) \{[(\alpha_1 - \Omega_1) \sin(\omega(t-t_1)) - \omega \cos(\omega(t-t_1))] / \\
& [(\alpha_1 - \Omega_1)^2 + \omega^2] - [(\alpha_1 + \Omega_1) \sin(\omega(t-t_1)) - \omega \cos(\omega(t-t_1))] / \\
& [(\alpha_1 + \Omega_1)^2 + \omega^2] + e^{(\Omega_1 - \alpha_1)(t-t_1)} [\omega/((\alpha_1 - \Omega_1)^2 + \omega^2)] - \\
& e^{-(\Omega_1 + \alpha_1)(t-t_1)} [\omega/((\alpha_1 + \Omega_1)^2 + \omega^2)] \} \quad (3.1.2)
\end{aligned}$$

for $t_1 \leq t \leq t_1 + D$, i.e., while the pulse is acting, and

$$\begin{aligned}
x(t; y_0, t_0) = & e^{-\alpha_1(t-t_0)} [A_0 \cosh(\Omega_1(t-t_0)) + B_0 \sinh(\Omega_1(t-t_0))] \\
& + (\beta/2\Omega_1) \{ e^{(\Omega_1 - \alpha_1)(t-t_1)} (e^{(\alpha_1 - \Omega_1)D} + 1.0) [\omega/((\alpha_1 - \Omega_1)^2 + \omega^2)] \\
& - e^{-(\Omega_1 + \alpha_1)(t-t_1)} (e^{(\alpha_1 + \Omega_1)D} + 1.0) [\omega/((\alpha_1 + \Omega_1)^2 + \omega^2)] \} \quad (3.1.3)
\end{aligned}$$

for $t \geq t_1 + D$ and $x < x_{02}$, i.e., after the pulse has ceased but

before the paper is struck, where $A_0 = x_{01} - F_0$, $B_0 = (y_0 + \alpha_1 A_0)/\Omega_1$,

and $\Omega_1 = \sqrt{1.0 + \alpha_1}$.

Based at (x_{02}, y_4, t_4) the solution to equation (2.1.7) is

$$x(t; y_4, t_4) = e^{-\alpha_1(t-t_4)} [A_4 \cosh(\Omega_1(t-t_4)) + B_4 \sinh(\Omega_1(t-t_4))] + F_0 \quad (3.1.4)$$

for $x_{01} < x < x_{02}$ where $y_4 < 0$, with $A_4 = x_{02} - F_0$, and $B_4 = (y_4 + \alpha_1 A_4)/\Omega_1$. This will be used for the return flight from the paper to the backstop.

Similarly the solution to the equation (2.1.8) based at (x_{02}, y_3, t_3) is

$$x(t; y_3, t_3) = e^{-\alpha_2(t-t_3)} [A_3 \cosh(\Omega_2(t-t_3)) + B_3 \sinh(\Omega_2(t-t_3))] + (1.0 + k^2)x_{02}/k^2 - F_0/k^2 \quad (3.1.5)$$

for $x \geq x_{02}$ where $A_3 = F_0/k^2 - x_{02}/k^2$, $B_3 = (y_3 + \alpha_2 A_3)/\Omega_2$, and

$\Omega_2 = \sqrt{k^2 - \alpha_2^2}$. This gives the dynamics during contact with the ribbon and paper.

For the case of n impacts per forcing cycle, the solutions to the governing equation (2.1.7) for the settle-out phase are

$$x(t; y_1, t_1) = e^{-\alpha_2(t-t_1)} [A_0 \cosh(\Omega_1(t-t_1)) + B_1 \sinh(\Omega_1(t-t_1))]$$

$$+ F_0 \quad (3.1.6)$$

where (t_1, y_1) is the point on the backstop at which time the mass leaves, and $B_1 = (y_1 + \alpha_1 A_0)/\Omega_1$. (It should be noted that the word "impacts" in this dissertation refer to impact against the backstop).

A periodic motion of one impact per forcing cycle will satisfy the following matching conditions:

$$x(t_3 ; y_0, t_0) = x_{02} \quad (3.1.7)$$

$$\dot{x}(t_3 ; y_0, t_0) = y_3 \quad (3.1.8)$$

$$x(t_4 ; y_3, t_3) = x_{02} \quad (3.1.9)$$

$$\dot{x}(t_4 ; y_3, t_3) = y_4 \quad (3.1.10)$$

$$x(t_5 ; y_4, t_4) = x_{01} \quad (3.1.11)$$

$$\dot{x}(t_5 ; y_4, t_4) = y_5 \quad (3.1.12)$$

$$y_0 = -r y_5 \quad (3.1.13)$$

$$t_5 - t_0 = T . \quad (3.1.14)$$

For the conditions of the existence of motion of period T with k impacts, equations (3.1.13) and (3.1.14) are rewritten as

$$y_0 = -r y_8 \quad (3.1.13a)$$

$$x(t_{2i+7} ; y_{2i+6}, t_{2i+6}) = x_{01} \quad (3.1.13b)$$

$$\dot{x}(t_{2i+7} ; y_{2i+6}, t_{2i+6}) = y_{2i+7} \quad (3.1.13c)$$

$$y_{2i+8} = -r y_{2i+8} \quad (3.1.13d)$$

$$t_{2i+8} - t_0 = T \quad (3.1.14a)$$

where $i = 0, 1, 2, \dots, k-2$, and T is the period of excitation. Then the corresponding periodic points of the mapping P_1 , when the Poincare section in equation (2.2.4) is adopted, can be written as

$$(\bar{t}+T, \bar{y}) = P_1^k(\bar{t}, \bar{y}). \quad (3.1.15)$$

If the Poincare map of the equation (2.2.2) is adopted, the corresponding fixed point can be written as

$$(\bar{x}, \bar{y}) = P^{t_0}(\bar{x}, \bar{y}) \quad (3.1.16)$$

since only one forcing period passes during the k impacts.

Solving equations (3.1.7) - (3.1.14) with solutions of equations (3.1.1) - (3.1.6) the periodic points corresponding to a specific forcing periods T with k impacts can be obtained. In this dissertation, due to the generally unstable behavior of period nT ($n > 1$) motions, we are mainly concerned with the period T motions with $k > 1$ impacts per forcing cycle. A computer generated plot of the resonance curves of periodic points \bar{y} versus forcing period T is shown in Figure 9. On the curves, solid lines represent stable motions and the dashed lines represent unstable motions. The values shown correspond to the \bar{y} component of the periodic points on the Poincare section of equation (2.2.4).

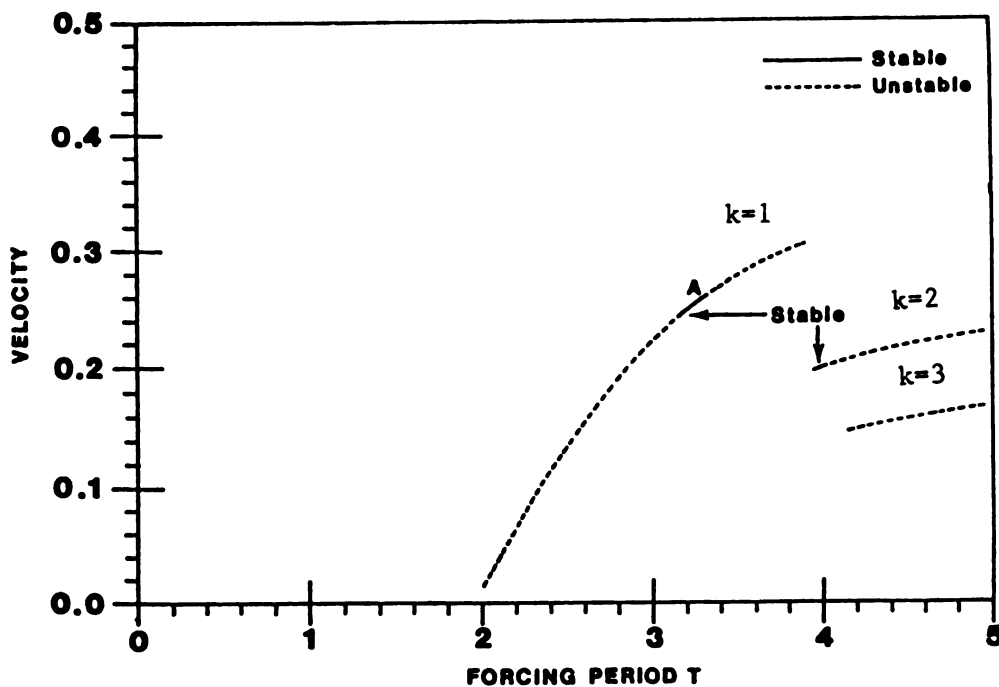


Figure 9. Resonance curves \bar{y} versus forcing period T .

The response curves shown in Figure 9 was generated by a numerical solution of the matching problem. In equation (3.1.7) t_3 cannot be analytically determined since it is the root of the transcendental equation. The same is true for t_4 and t_5 . However, the local solutions for equations (3.1.7)-(3.1.12) are known explicitly. We assume that the pulse is only acting when the armature is not in contact with the paper. This must be verified from simulations, as seen in Figure 6 for example. From the periodic conditions for one impact per forcing cycle in equations (3.1.7)-(3.1.14) and their local solutions there are 8 unknowns ($t_0, y_0, t_3, y_3, t_4, y_4, t_5, y_5$) in these 8 equations. Solving these equations by numerical methods, we obtain the periodic points in Σ for various parameters. By following the same procedure we can obtain the periodic points for k impacts per forcing cycle in parameter region as shown in Figure 9. An IMSL routine, ZSPOW, was used to solve these equations [44].

3.2 Stability Analysis

For the stability nature of a period motion, we choose a point on the orbit as the periodic point by constructing a Poincare section as described in section 2.2. For convenience a Poincare section is chosen at the point where the pulse is applied, i.e., Σ^{t_0} is used. In the following analysis, we choose the point of equation (3.1.16) as the periodic point with the Poincare section of equation (2.2.2). The

Poincare section chosen here is different from the section of equation (2.2.4) which was used in [26-30]. However, the approach taken here is similar and is equivalent to those in [23-24].

A small deviation from the fixed point is considered. After n cycles under the action of mapping P , the system is stable if $\lim_{n \rightarrow \infty} DP^n = 0$, where DP is the linearization of P about the fixed point. Equivalently, $|\lambda_i| < 1$ where λ_i are the eigenvalues of DP . In the following we consider two impacts per forcing cycle as an example. The stability of k impacts per forcing cycle has been analyzed by following a similar procedure. It is assumed that $\dot{x} < v_1$ for all impacts.

Referring to Figure 6(b), it is seen that there are 8 pieces of a periodic trajectory which form one cycle with two impacts at the backstop. Hence DP (with P^{t_0} written simply as P) can be written using the chain rule as :

$$DP = DP_{10}DP_{07}DP_{76}DP_{65}DP_{54}DP_{43}DP_{32}DP_{21} \quad (3.2.1)$$

where the P_{ij} are the components of the map for the respective components of the trajectory. The details of calculating the components of each DP_{ij} are given as follows. From point 1 to point 2 the solution to the equation of motion based at point 1 (x_1, y_1, t_1) is

$$x(t; x_1, y_1, t_1) = e^{-\alpha_1(t-t_1)} [A_1 \cosh(\Omega_1(t-t_1)) + B_1 \sinh(\Omega_1(t-t_1))]$$

$$\begin{aligned}
& + F_0 + (\beta/2\Omega_1) \{ [(\alpha_1 - \Omega_1) \sin(\omega(t-t_1)) - \omega \cos(\omega(t-t_1))] / \\
& [(\alpha_1 - \Omega_1)^2 + \omega^2] - [(\alpha_1 + \Omega_1) \sin(\omega(t-t_1)) - \omega \cos(\omega(t-t_1))] / \\
& [(\alpha_1 + \Omega_1)^2 + \omega^2] + e^{\frac{(\Omega_1 - \alpha_1)(t-t_1)}{[\omega/((\alpha_1 - \Omega_1)^2 + \omega^2)]}} - \\
& e^{\frac{-(\Omega_1 + \alpha_1)(t-t_1)}{[\omega/((\alpha_1 + \Omega_1)^2 + \omega^2)]}} \} \quad (3.2.2)
\end{aligned}$$

where $A_1 = x_1 - F_0$, $B_1 = (y_1 + \alpha_1 A_1)/\Omega_1$.

The point 2 (x_2, y_2, t_2) , at which the sine pulse ceases, is determined by

$$x(t_2 ; x_1, y_1, t_1) = x_2 \quad (3.2.3)$$

$$y(t_2 ; x_1, y_1, t_1) = y_2 \quad (3.2.4)$$

where $t_2 = t_1 + D$, and D is the duration of the sine pulse.

A small perturbation of $(x_1, y_1) \in \Sigma^{t_0}$ will cause a variation in point 2. Taking $\frac{\partial}{\partial x_1}$ and $\frac{\partial}{\partial y_1}$ of equation (3.2.3) respectively and using equation (3.2.2) we obtain

$$\frac{\partial x_2}{\partial x_1} = e^{-\alpha_1 D} \left[\cosh(\Omega_1 D) + \frac{\alpha_1}{\Omega_1} \sinh(\Omega_1 D) \right] \quad (3.2.5)$$

$$\frac{\partial x_2}{\partial y_1} = e^{-\alpha_1 D} \left[\frac{1}{\Omega_1} \sinh(\Omega_1 D) \right] . \quad (3.2.6)$$

Next taking $\frac{\partial}{\partial x_1}$ and $\frac{\partial}{\partial y_1}$ of equation (3.2.4) respectively and using the time derivative of equation (3.2.2) we obtain

$$\frac{\partial y_2}{\partial x_1} = e^{-\alpha_1 D} \left[\Omega_1 - \frac{\alpha_1^2}{\Omega_1} \right] \sinh(\Omega_1 D) \quad (3.2.7)$$

$$\frac{\partial y_2}{\partial y_1} = e^{-\alpha_1 D} \left[\cosh(\Omega_1 D) - \frac{\alpha_1}{\Omega_1} \sinh(\Omega_1 D) \right] . \quad (3.2.8)$$

From point 2 to point 3 the solution to the motion based at (x_2, y_2, t_2) is

$$\begin{aligned} x(t ; x_2, y_2, t_2) = & e^{-\alpha_1(t-t_2)} [A_2 \cosh(\Omega_1(t-t_2)) + B \sinh(\Omega_1(t-t_2))] \\ & + F_0 \end{aligned} \quad (3.2.9)$$

where $A_2 = x_2 - F_0$, $B_2 = (y_2 + \alpha_1 A_2)/\Omega_1$.

The point (x_{02}, y_3, t_3) can be determined from

$$x(t_3; x_2, y_2, t_2) = x_{02} \quad (3.2.10)$$

$$\dot{x}(t_3; x_2, y_2, t_2) = y_3 \quad (3.2.11)$$

A small perturbation to point 2 will cause a variation in (t_3, y_3) since x_{02} remains unchanged. Thus (t_3, y_3) are dependent on (x_2, y_2) . It should be noted that $t_2 = t_1 + D$ is also kept constant.

Taking $\frac{\partial}{\partial x_2}$ and $\frac{\partial}{\partial y_2}$ of equation (3.1.10) respectively and using the time derivative of equation (3.2.9) we get

$$\frac{\partial t_3}{\partial x_2} = -\frac{1}{y_3} \left(e^{-\alpha_1(t_3-t_2)} \left[\cosh(\Omega_1(t_3-t_2)) + \frac{\alpha_1}{\Omega_1} \sinh(\Omega_1(t_3-t_2)) \right] \right) \quad (3.2.12)$$

$$\frac{\partial t_3}{\partial y_2} = -\frac{1}{y_3} \left[e^{-\alpha_1(t_3-t_2)} \frac{1}{\Omega_1} \sinh(\Omega_1(t_3-t_2)) \right] \quad (3.2.13)$$

Next taking $\frac{\partial}{\partial x_2}$ and $\frac{\partial}{\partial y_2}$ of equation (3.2.11) respectively and using the time derivative of equation (3.2.9) and equation (3.1.7) we get

$$\begin{aligned}
\frac{\partial y_3}{\partial x_2} = & \left[\frac{F_0 - x_{02}}{y_3} + \alpha_1 \right] e^{-\alpha_1(t_3 - t_2)} \left[\cosh(\Omega_1(t_3 - t_2)) + \frac{\alpha_1}{\Omega_1} \right. \\
& \left. \sinh(\Omega_1(t_3 - t_2)) \right] + e^{-\alpha_1(t_3 - t_2)} \left[\Omega_1 \sin(\Omega_1(t_3 - t_2)) + \right. \\
& \left. \alpha_1 \cosh(\Omega_1(t_3 - t_2)) \right]
\end{aligned} \tag{3.2.14}$$

$$\begin{aligned}
\frac{\partial y_3}{\partial y_2} = & \left[\frac{F_0 - x_{02}}{y_3} + \alpha_1 \right] e^{-\alpha_1(t_3 - t_2)} \left[\frac{1}{\Omega_1} \sinh(\Omega_1(t_3 - t_2)) \right] \\
& + e^{-\alpha_1(t_3 - t_2)} \cosh(\Omega_1(t_3 - t_2)).
\end{aligned} \tag{3.2.15}$$

From point 3 to point 4 the solution to the motion is given by equation (3.1.5). The point 4, (x_{02}, y_4, t_4) , is determined by

$$x(t_4; x_{02}, y_3, t_3) = x_{02} \tag{3.2.16}$$

$$\dot{x}(t_4; x_{02}, y_3, t_3) = y_4 \tag{3.2.17}$$

where x_{02} is constant. A small perturbation to (t_3, y_3) will then cause a variation in (t_4, y_4) .

Taking $\frac{\partial}{\partial t_3}$ and $\frac{\partial}{\partial y_3}$ of equation (3.2.16) respectively and using equation (3.1.5) we get

$$\frac{\partial t_4}{\partial t_3} = 1.0 \quad (3.2.18)$$

$$\frac{\partial t_4}{\partial y_3} = - e^{-\alpha_2(t_4-t_3)} \frac{1}{\Omega_2 y_4} \sin(\Omega_2(t_4-t_3)) \quad (3.2.19)$$

Taking $\frac{\partial}{\partial t_3}$ and $\frac{\partial}{\partial y_3}$ of equation (3.2.17) respectively and using the first time derivative of equation (3.1.5) and equations (2.1.8), (3.2.18) and (3.2.19) we get

$$\frac{\partial y_4}{\partial t_3} = 0.0 \quad (3.2.20)$$

$$\begin{aligned} \frac{\partial y_4}{\partial y_3} = & \left[\frac{F_0 - x_{02}}{y_4} + \alpha_2 \right] e^{-\alpha_2(t_4-t_3)} \frac{1}{\Omega_2} \sin(\Omega_2(t_4-t_3)) \\ & + e^{-\alpha_2(t_4-t_3)} \cos(\Omega_2(t_4-t_3)). \end{aligned} \quad (3.2.21)$$

By similar procedure and calculation we can get the components of DP_{45} as follows:

$$\frac{\partial t_5}{\partial t_4} = 1.0 \quad (3.2.22)$$

$$\frac{\partial t_5}{\partial y_4} = - e^{-\alpha_1(t_5-t_4)} \frac{1}{\Omega_1 y_5} \sinh(\Omega_1(t_5-t_4)) \quad (3.2.23)$$

$$\frac{\partial y_5}{\partial t_4} = 0.0 \quad (3.2.24)$$

$$\begin{aligned} \frac{\partial y_5}{\partial y_4} = & \left[\frac{F_0 - x_{01}}{y_5} + \alpha_1 \right] e^{-\alpha_1(t_5-t_4)} \frac{1}{\Omega_1} \sinh(\Omega_1(t_5-t_4)) \\ & + e^{-\alpha_1(t_5-t_4)} \cosh(\Omega_1(t_5-t_4)). \end{aligned} \quad (3.2.25)$$

From point 5 to 6 the first impact at the backstop occurs. By equation (2.1.9) and (2.1.10), we can easily get the components of DP_{56} as follows

$$\frac{\partial t_6}{\partial t_5} = 1.0 \quad (3.2.26)$$

$$\frac{\partial t_6}{\partial y_5} = 0.0 \quad (3.2.27)$$

$$\frac{\partial y_6}{\partial t_5} = 0.0 \quad (3.2.28)$$

$$\frac{\partial y_6}{\partial y_5} = -\delta - 2\alpha y_5. \quad (3.2.29)$$

From point 6 to point 7 the solution to the motion is given by equation (3.1.6). the point 7, (x_0, y_7, t_7) , is determined by

$$x(t_7 ; x_0, y_6, t_6) = x_0 \quad (3.2.30)$$

$$y(t_7 ; x_0, y_6, t_6) = y_7 \quad (3.2.31)$$

where y_7 can be obtained from equation (3.2.31) after solving equation (3.2.30) for t_7 . A small perturbation to t_6, y_6 will cause a variation in t_7 and y_7 . Taking $\frac{\partial}{\partial t_6}$ and $\frac{\partial}{\partial y_6}$ of equation (3.2.30) respectively and using equation (3.1.6) we obtain

$$\frac{\partial t_7}{\partial t_6} = 1.0 \quad (3.2.32)$$

$$\frac{\partial t_7}{\partial y_6} = - e^{-\alpha_1(t_7-t_6)} \frac{1}{\Omega_1 y_7} \sinh(\Omega_1(t_7-t_6)) . \quad (3.2.33)$$

Taking $\frac{\partial}{\partial t_6}$ and $\frac{\partial}{\partial y_6}$ of equation (3.2.31) respectively and using the first time derivative of equation (3.1.6) and equations (2.1.7), (3.2.32) and (3.2.33) we get

$$\frac{\partial y_7}{\partial t_6} = 0.0 \quad (3.2.34)$$

$$\begin{aligned} \frac{\partial y_7}{\partial y_6} = & \left[\frac{F_0 - x_{01}}{y_7} + \alpha_1 \right] e^{-\alpha_1(t_7 - t_6)} \frac{1}{\Omega_1} \sinh(\Omega_1(t_7 - t_6)) \\ & + e^{-\alpha_1(t_7 - t_6)} \cosh(\Omega_1(t_7 - t_6)). \end{aligned} \quad (3.2.35)$$

From point 7 to point 0 the second impact at the backstop occurs. The components of DP_{07} are

$$\frac{\partial t_0}{\partial t_7} = 1.0 \quad (3.2.36)$$

$$\frac{\partial t_0}{\partial y_7} = 0.0 \quad (3.2.37)$$

$$\frac{\partial y_0}{\partial t_7} = 0.0 \quad (3.2.38)$$

$$\frac{\partial y_0}{\partial y_7} = -\delta - 2\alpha y_7. \quad (3.2.39)$$

From point 0 to point 1, a small perturbation to (t_0, y_0) will cause a variation in (x_1, y_1) . The point (x_1, y_1, t_1) can be determined from

$$x(\bar{t}_1 ; x_{01}, y_0, t_0) = x_1 \quad (3.2.40)$$

$$\dot{x}(\bar{t}_1 ; x_{01}, y_0, t_0) = y_1 \quad (3.2.41)$$

where $\bar{t}_1 = t_1 \pmod{T}$.

Taking $\frac{\partial}{\partial t_0}$ and $\frac{\partial}{\partial y_0}$ of equation (3.2.40) respectively and using equation (3.1.1) we obtain

$$\frac{\partial x_1}{\partial t_0} = -y_1 \quad (3.2.42)$$

$$\frac{\partial x_1}{\partial y_0} = e^{-\alpha_1(\bar{t}_1 - t_0)} \frac{1}{\Omega_1} \sinh(\Omega_1(\bar{t}_1 - t_0)) . \quad (3.2.43)$$

Taking $\frac{\partial}{\partial t_0}$ and $\frac{\partial}{\partial y_0}$ of equation (3.2.41) respectively and using the first time derivative of equation (3.1.1) and equations (3.2.42), (3.2.43) and (3.1.1) we get

$$\frac{\partial y_1}{\partial t_0} = 2\alpha_1 y_1 - x_1 + F_0 \quad (3.2.44)$$

$$\frac{\partial y_1}{\partial y_0} = e^{-\alpha_1(\bar{t}_1 - t_0)} [\cosh(\Omega_1(\bar{t}_1 - t_0)) - \frac{\alpha_1}{\Omega_1} \sinh(\Omega_1(\bar{t}_1 - t_0))] . \quad (3.2.45)$$

From above above, DP can be written as

$$DP = \begin{bmatrix} \frac{\partial(x_1, y_1)}{\partial(t_0, y_0)} & \frac{\partial(t_0, y_0)}{\partial(t_7, y_7)} & \frac{\partial(t_7, y_7)}{\partial(t_6, y_6)} & \frac{\partial(t_6, y_6)}{\partial(t_5, y_5)} & \frac{\partial(t_5, y_5)}{\partial(t_4, y_4)} \\ \frac{\partial(t_4, y_4)}{\partial(t_3, y_3)} & \frac{\partial(t_3, y_3)}{\partial(x_2, y_2)} & \frac{\partial(x_2, y_2)}{\partial(x_1, y_1)} & & \end{bmatrix} \quad (3.2.46)$$

Performing the matrix multiplication of equation (3.2.46) and using the periodic points obtained in section 3.2, we can obtain the matrix DP evaluated on the periodic point. Then the eigenvalues of DP can be written in term of \bar{D} , the determinant of DP and \bar{T} , the trace of DP, as

$$\lambda_{1,2} = \frac{\bar{T}}{2} \pm \sqrt{\left(\frac{\bar{T}}{2}\right)^2 - \bar{D}} \quad (3.2.47)$$

which determine the stability of (x_1, y_1) and the correspond periodic motion.

Variation of the system parameters will cause the fixed point and its associated eigenvalues to move. If an eigenvalue passes through the unit cycle in the complex plane, i.e., $|\lambda| = 1$, a stability change and an associated bifurcation occur. Bifurcation conditions on the system parameters are determined by the equations

$$\bar{D} \mp \bar{T} + 1 = 0 \quad (3.2.48)$$

corresponding to $\lambda = \pm 1$ respectively. No Hopf bifurcations involving complex eigenvalues occur in this system since $\bar{D} < 1$ as is demonstrated below.

From the curves shown in Figure 9, as the forcing period T is varied, the eigenvalues corresponding to a periodic point change. At point A one of the eigenvalues will be equal to -1, in our case, and a period doubling bifurcation occurs. The periodic point \bar{y} of point A is called a bifurcation point and denoted \bar{y}_{bif} . This can be obtained by solving equation (3.2.48) and (3.1.7) - (3.1.14) numerically. The method is similar to the one described in section 3.2 for obtaining the period points in Poincare section Σ . We only add one unknown \bar{y}_{bif} and one equation of (3.2.48). In this bifurcation the stable motion of period T becomes unstable and a stable motion of period $2T$ appears. Fig 10(a) shows flip bifurcation curves of forcing period T (corresponding to the bifurcation point \bar{y}_{bif}) versus the backstop material factor α . It is observed that as α is increased, i.e., as the damping of the backstop is increased, the forcing period T corresponding to \bar{y}_{bif} will be decreased. This indicates the print hammer may be excited at higher forcing frequencies with a stable periodic motion by increasing the damping of the backstop. Also, increasing the damping of the backstop reduces the settle-out time, further discussion of these issues follows in next section. A similar

procedure indicates that as the system damping during free flight, α_1 , is increased the change in forcing period T at the bifurcation is small as shown in Figure 10(b). This indicates the effect of changing α_1 is not significant.

Similarly the bifurcation point \bar{y}_{bif} for k impacts per forcing cycle can be determined by following the procedure described above. It is found that there are no stable regions for periodic motions with $k > 3$, so \bar{y}_{bif} does exist for $k > 3$.

3.3 Simulation and Observations

Using results of digital simulations we can check the validity of our solutions to the equations of motion, periodic points, and bifurcation points. Also, chaotic motions and other responses can be explored through simulation. Figures 6(a) and 6(b) show the plots of phase portraits with one and two impacts per forcing cycle respectively. It was determined that the fixed points corresponding to the motions in Figures 6(a) and 6(b) are exactly coincident with their respective fixed points as predicated by the analysis.

Figure 11 indicates a flip bifurcation. Figure 11(a) shows a phase portrait whose eigenvalue is close to negative one. Figure 11(b) shows the plot of phase portrait with period $2T$, the motion has a period twice the period of the forcing period T . As we continuously change the parameter T , we obtain the period $4T$ motion shown in Figure

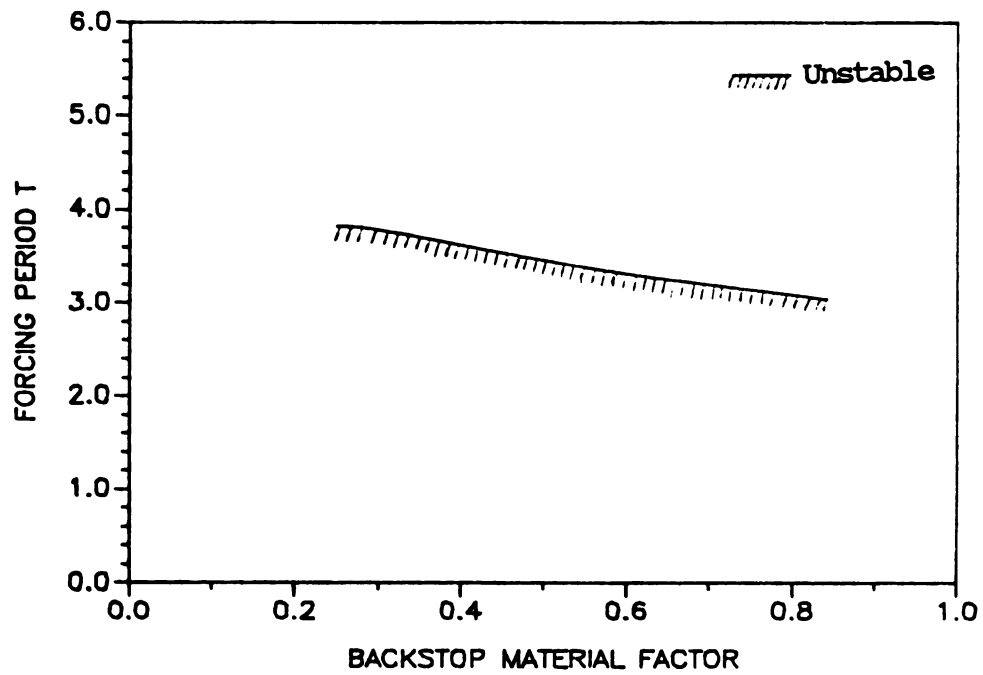


Figure 10(a) Flip bifurcation curve for one impact at backstop

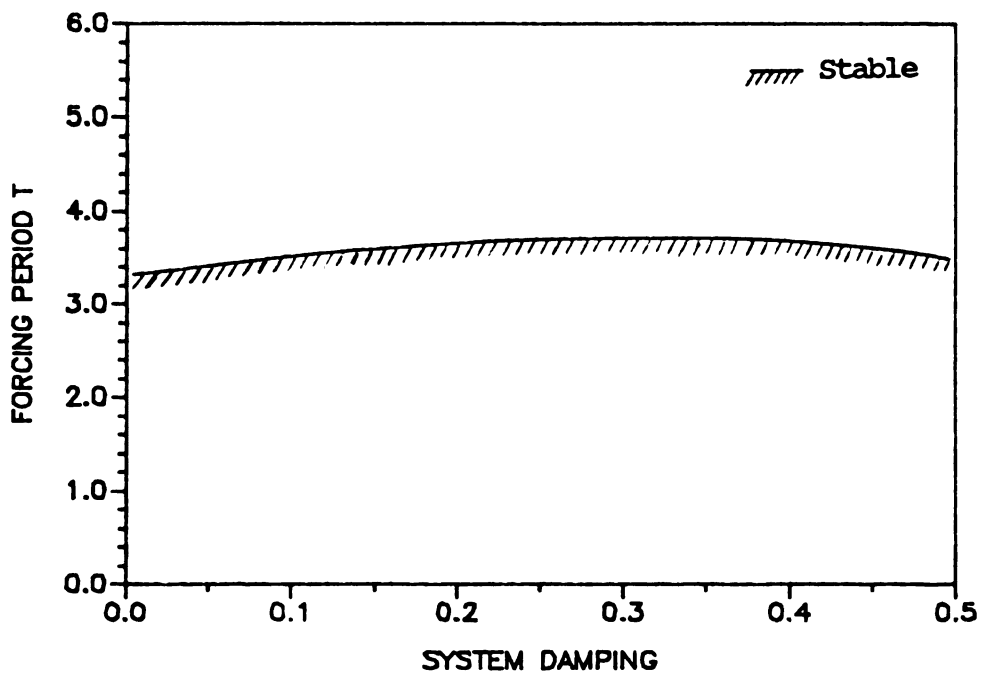


Figure 10(b). Flip bifurcation curve for one impact at backstop

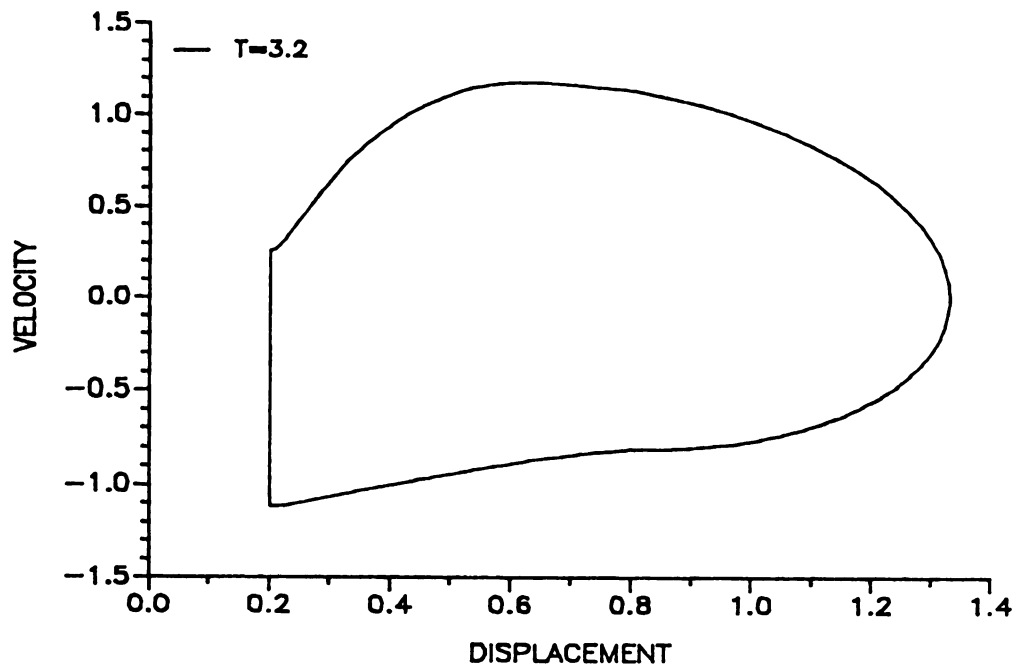


Figure 11(a). Period 1 orbit, $T=3.2$

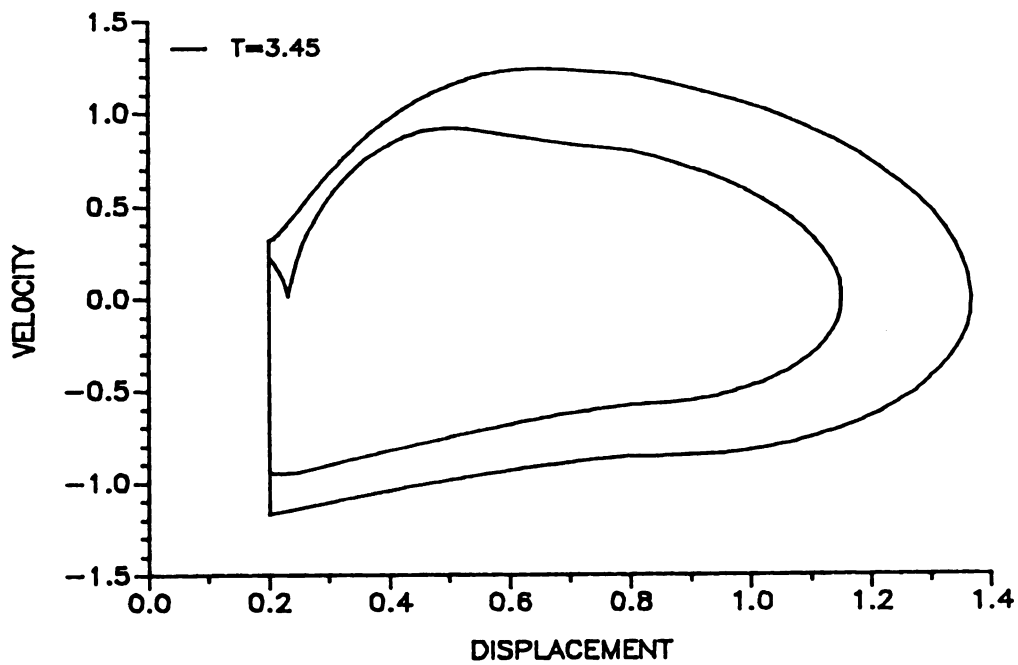


Figure 11(b) Period 2 orbit, $T=3.45$

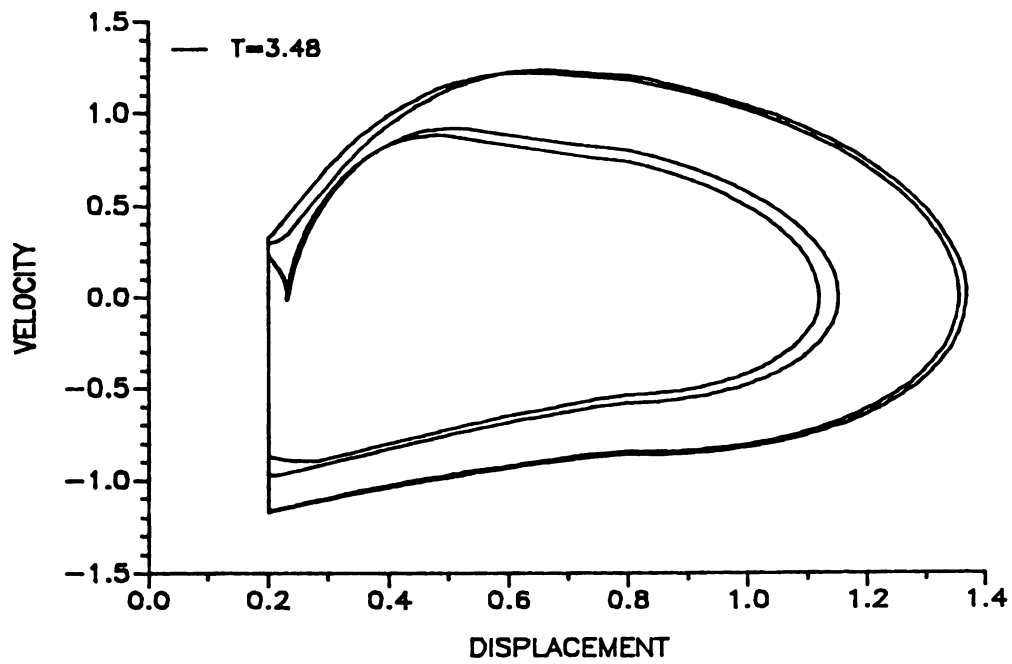


Figure 11(c). Period 4 orbit, $T=3.48$

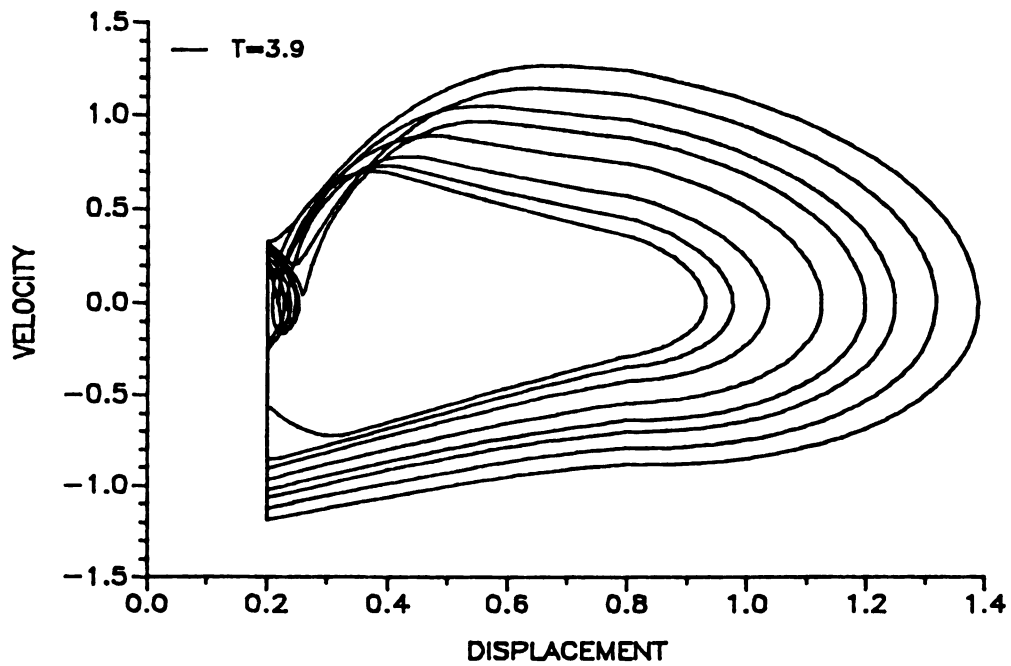


Figure 11(d) Chaotic motion, $T=3.9$

11(c), and finally a chaotic motion occurs as shown in Figure 11(d). The simulations indicate that as the forcing frequency is varied from $T = 3.2$ to $T = 3.45$, a flip bifurcation occurs. Checking the bifurcation curve in Figure 10, we can obtain the corresponding forcing frequency at the bifurcation which is equal to $T \approx 3.31$.

Since the system is excited by the periodic sine pulses of period T , the time t at which the armature leaves the backstop can be replaced with the phase ϕ , $\phi = t \bmod (T)$. This is convenient for describing orbits in Σ_1 . Figure 12 depicts the points (ϕ, y) in Σ_1 corresponding to the motions shown in Figure 11. It is observed that a slight change in phase ϕ causes a variation in the motion as shown in Figure 11(b) and Figure 12(b). It indicates that a flip bifurcation will affect print quality, i.e., dots will alternate between two values of maximum print force causing nonuniform printing.

In Figure 9 between the stable region represented by solid curves there exist many unstable regions represented by the dashed curves. It should be noted that one end-point of the solid curve segment is the bifurcation point discussed above and the other end point of a solid curve has been determined by simulation. At such point an orbit in phase portrait hits the backstop with zero impact velocity, i.e., a degenerate impact occurs and a motion of n impacts per forcing cycle undergoes a "transition" and becomes a motion of $n-1$ impacts per cycle. It undergoes a complicated sequence of chaotic motions and flip bifurcations in that transition [26,35]. By using the iterates of the Poincare map, i.e., plotting all points (x_1, y_1)

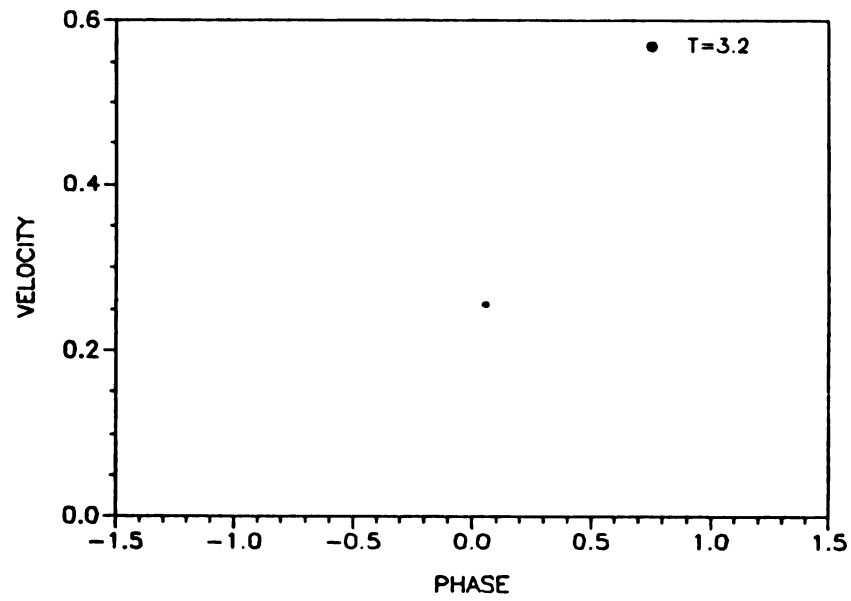


Figure 12(a) Period point of period 1, $T=3.2$

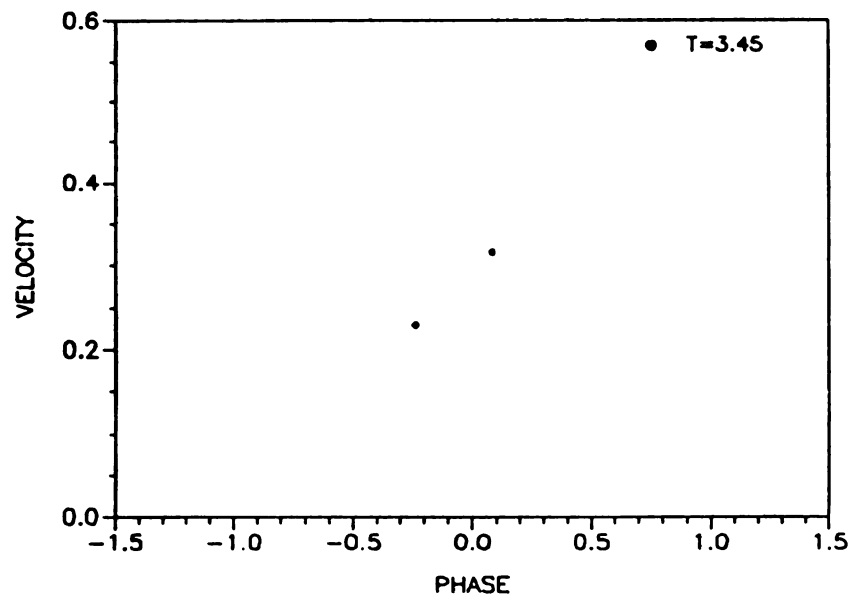


Figure 12(b) Periodic points of period 2, $T=3.45$

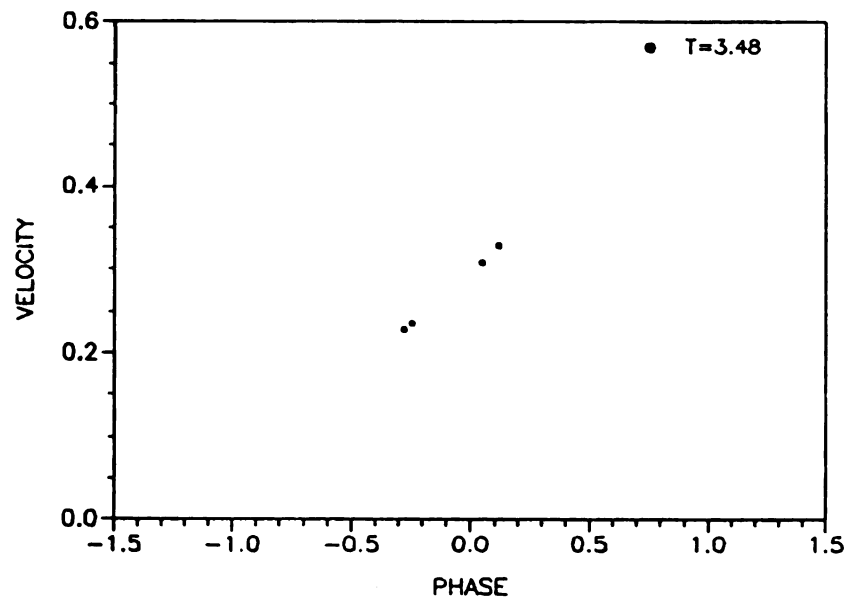


Figure 12(c) Periodic points of period 4 orbit, $T=3.48$

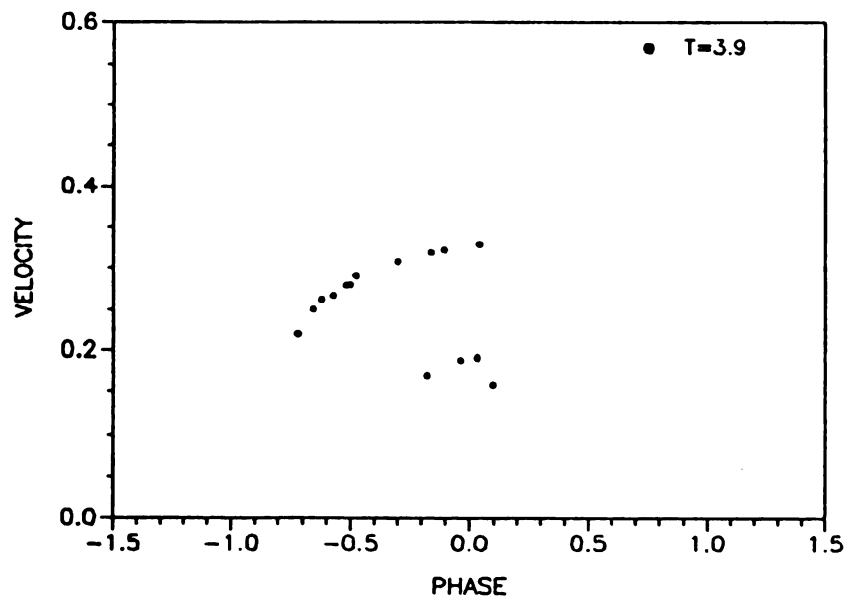


Figure 12(d) Chaotic motion in Σ , $T=3.9$

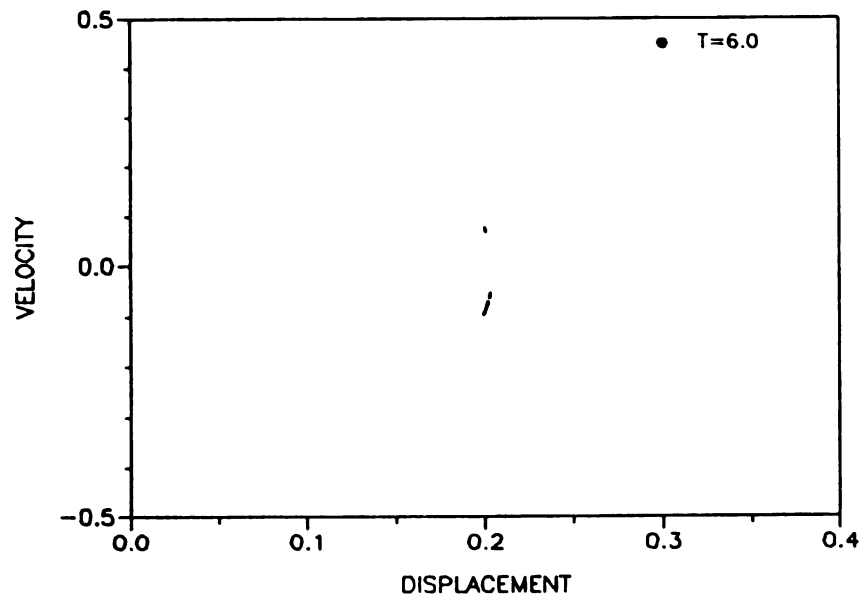


Figure 13(a) Poincare plot, $T=6.0$

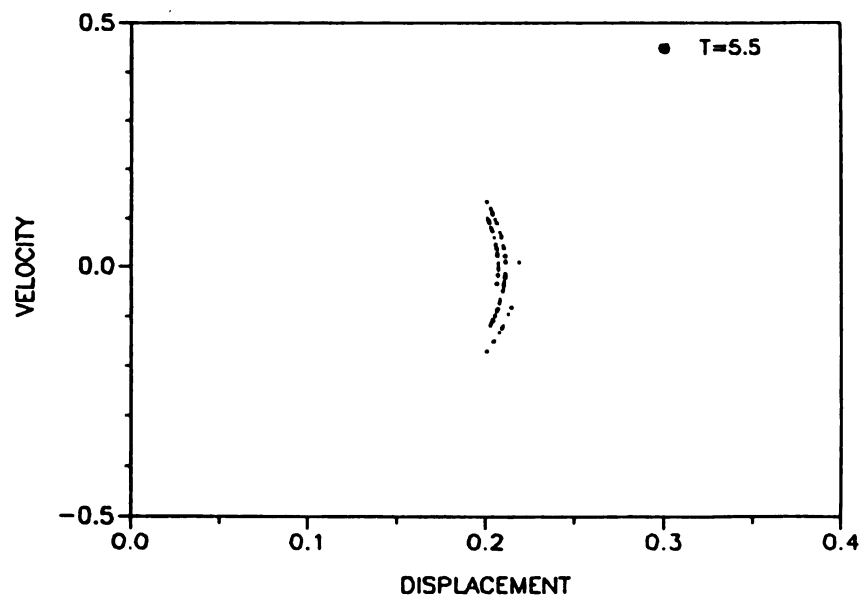


Figure 13(b) Poincare plot, $T=5.5$

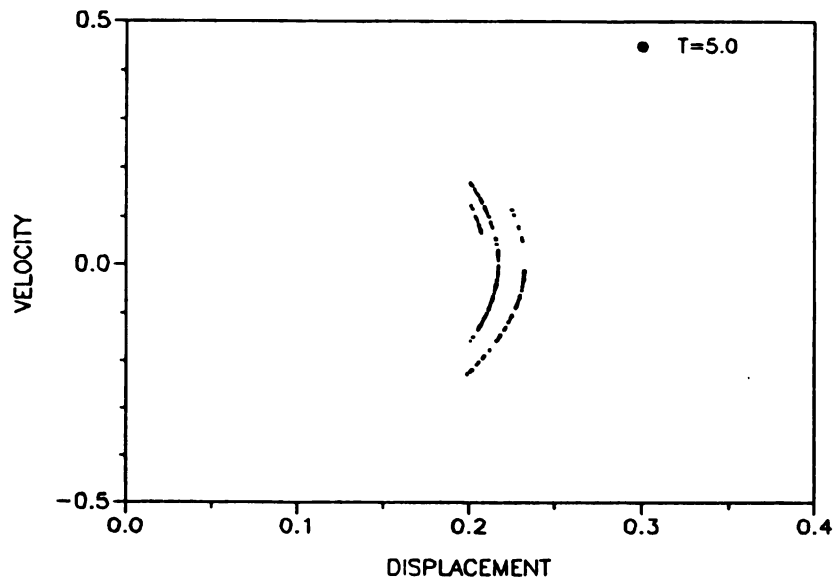


Figure 13(c) Poincare plot, $T=5.0$

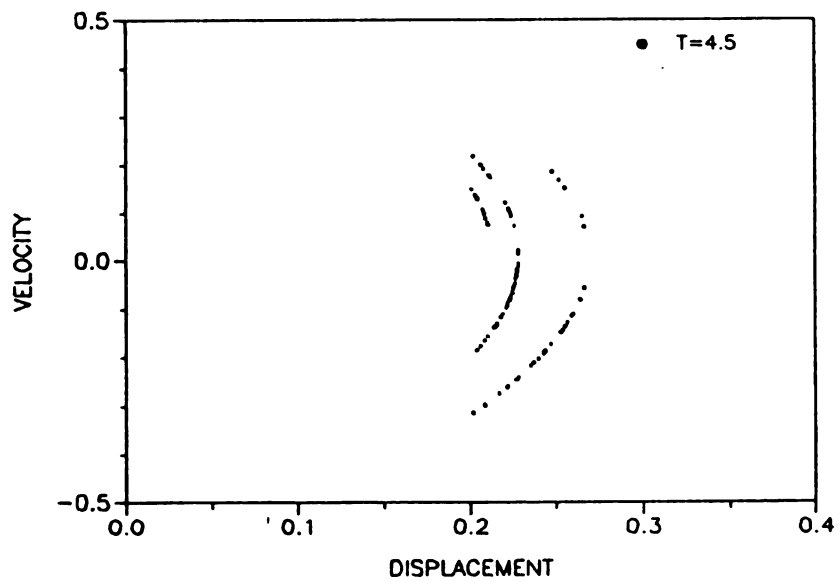


Figure 13(d) Poincare plot, $T=4.5$

which belong to Poincare section Σ^{t_0} of equation (2.2.2), we can describe the behavior of these unstable motions. Figure 13 shows Poincare plots for chaotic motions at different forcing periods. It is found that as the forcing period is increased, the phase points converge to the point $(x_1 = x_{01})$, i.e., to the rest position at the backstop.

Figures 14(a), (b) and (c) show a Poincare plot, a phase plane and a plot of the displacement versus time at the same parameter values, respectively, with a forcing frequency near that of "buzz

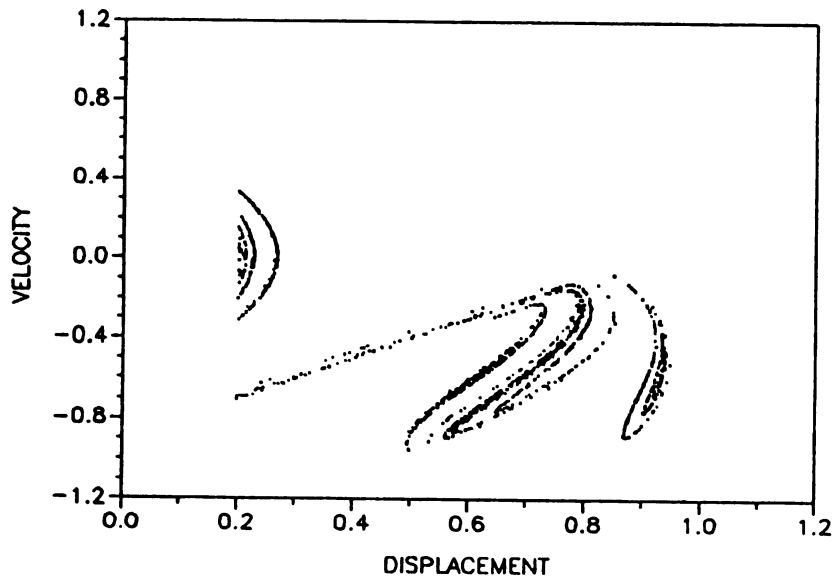


Figure 14(a) A Poincare plot, $T=2.5$

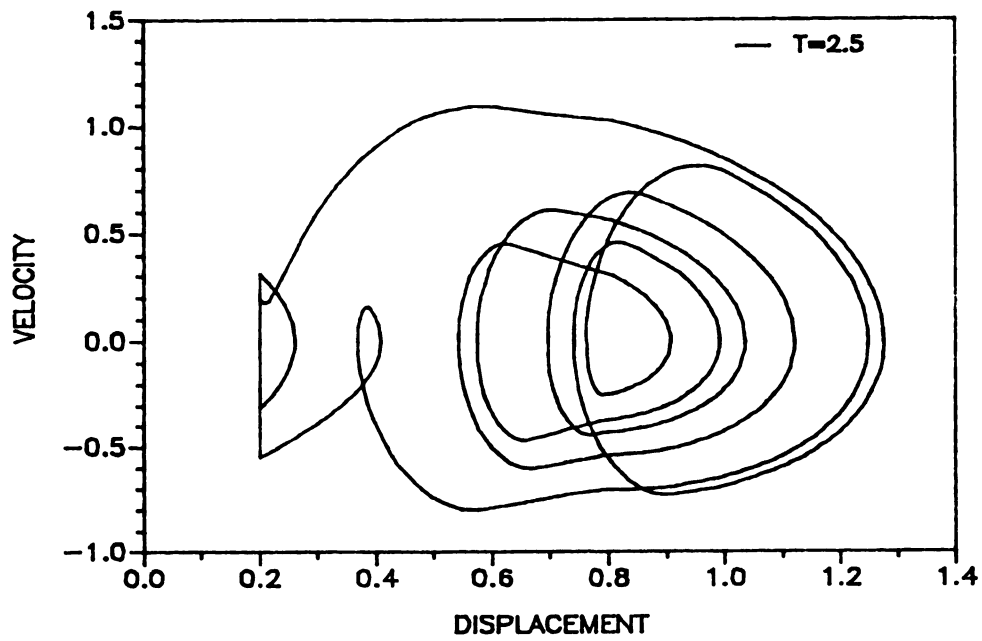


Figure 14(b) A chaotic motion, $T=2.5$

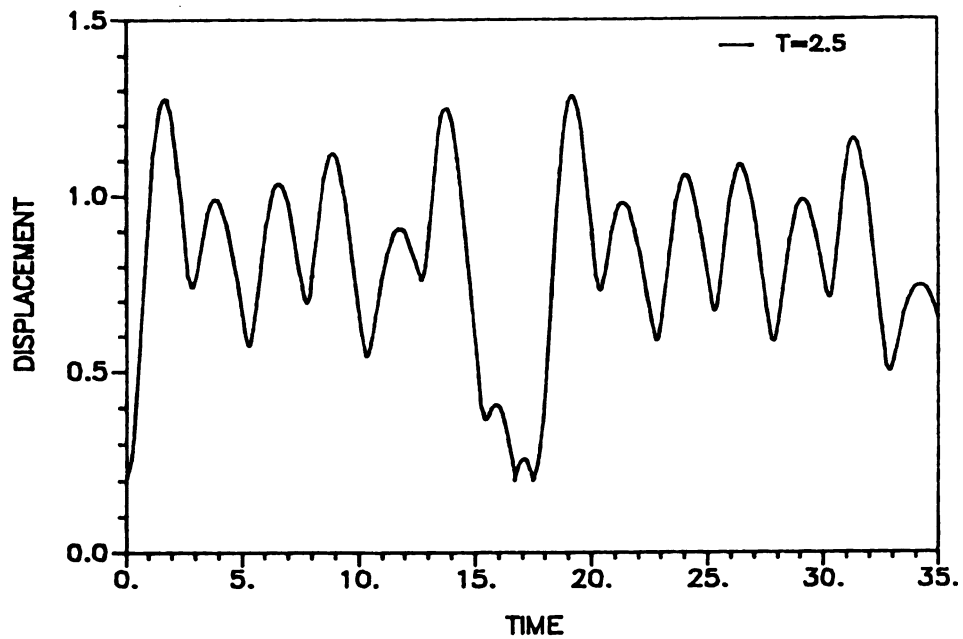


Figure 14(c) A plot of displacement vs. time, $T=2.5$

printing" [10]. A buzz printing mode is a behavior of motion at high frequency in which the hammer never returns to the backstop, and print forces are not large enough to produce acceptable print quality. This motion is typical of the chaotic motions that occur when the system is driven too rapidly.

It should be noted that the forcing in actual printers is not periodic, and Hendriks [10] pointed out that the motion of the hammer is extremely sensitive to the timing of subsequent refirings. In order to avoid interaction from rebound, the minimum forcing period T of the print hammer is set to be sufficiently large such that $y \approx 0$ at refire. Some works related to the improvement of performance have been indicated in [10-22]. It has also been observed that increasing the pre-load during settle-out phase will improve the performance. A open-loop control strategy which increases the operating speed will be discussed in next Chapter.

By using our simple model and carrying out analysis and simulations we have determined the influence of various parameters on the printer's performance. A plot of settle-out time versus pre-load is shown in Figure 15, this plot was obtained by gradually increasing the pre-load during the phase between the time that the hammer leaves the paper and the time of the next pulse. Figure 16 shows a plot of settle -out time versus the backstop material factor. The "ideal" settle-out time is the duration between the instant the armature leaves the paper and the time at which it comes to the rest position ($x=0.2$, $y=0.0$). For convenience in simulations we let the settle-out time be the time between the armature leaving the paper and settling

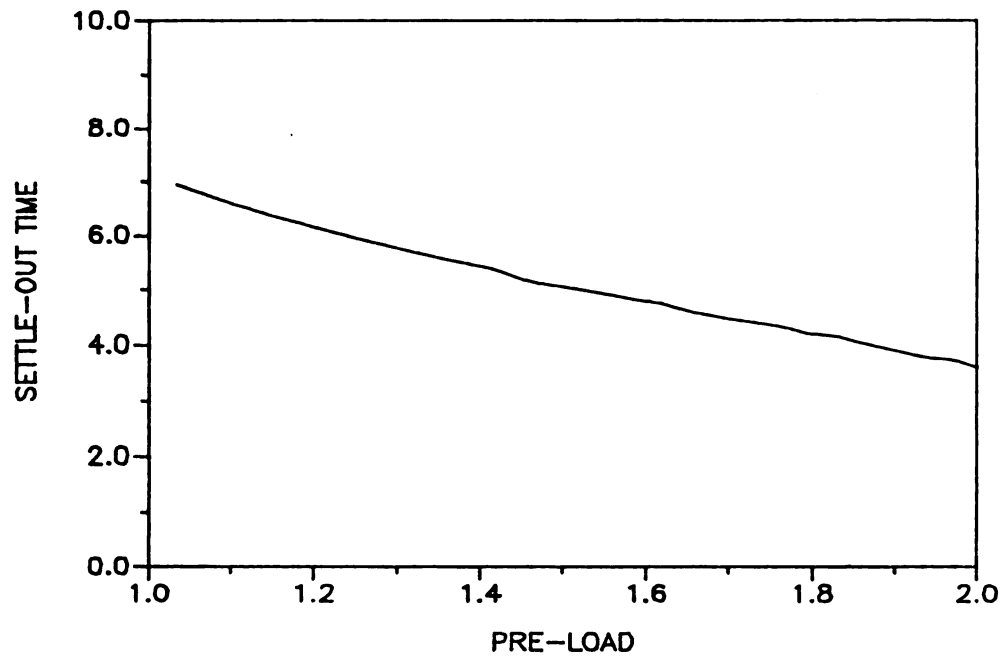


Figure 15. A plot of settle-out time vs. preload

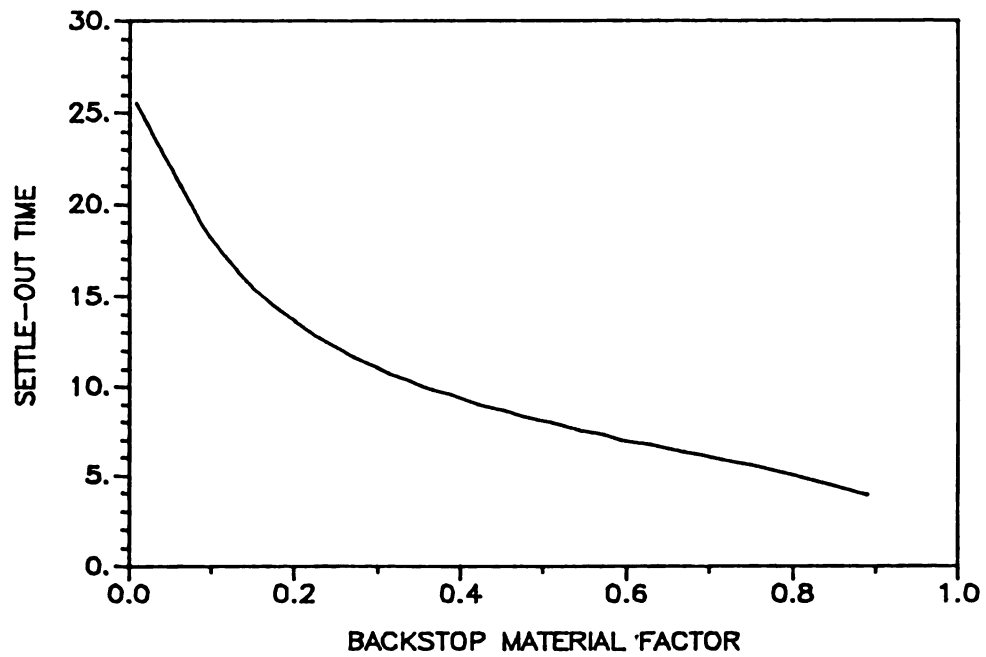


Figure 16. A plot of settle-out time vs. backstop material factor α

into the region ($x \approx 0.2$, $y < 0.04$). These graphs show that an increase in the backstop material damping and/or the pre-load during settle-out phase will quickly send the armature towards the rest position and subsequent refirings can take place nearly immediately. Note that refiring during settle-out, when the armature is very near the rest position, usually results in good print quality. By increasing the preload or the backstop material damping the impact printer can be operated at higher frequencies and the performance is improved. We will demonstrate this by using a control method to increase the preload in next Chapter. It is interesting to note that increasing the spring stiffness also reduces the settle-out time. However, the forces required for the permanent magnet and of the excitation would need to be likewise increased.

3.4 Chaotic Dynamics of the System

It is interesting to note that the Poincare points in Figures 13 and 14 tend to lie on a set of curves. This is referred to as a strange attractor [39]. Very similar attractors were also observed by Hendriks [10]. Both show that as the forcing period T is reduced the attractor "grows" and there is wide variation in initial conditions provided for refiring.

An attractor is an attracting set which contains a dense orbit [39]. An attracting set is an invariant set $A \in \mathbb{R}^n$ for which there exists some neighborhood U of A such that for all $x \in U$, solution

trajectories $\Phi(x,t)$ remain in U for all $t \geq 0$ and $\Phi(x,t) \rightarrow A$ as $t \rightarrow \infty$. It should be noted that an attracting set is not necessarily an attractor. The strange attractor is an attractor with some special properties. Observable chaotic motions in nonlinear systems correspond with the occurrence of a strange attractor in the phase space. A chaotic motion is an irregular, deterministic, and bounded motion with wide-band spectrum and displays sensitive dependence on initial conditions. As system parameters are varied, a periodic motion may pass through a series of bifurcations which results in a chaotic motion, as in the period doubling cascade. However, this is only part of the picture, global behavior is the source of the chaos.

Chaotic motions usually evolve from global bifurcations of a saddle type periodic motion for which the associated stable and unstable manifolds intersect transversely leading to Smale horseshoes (see Guckenheimer and Holmes [39], Shaw and Holmes [26], or Shaw [29] for details). The stable (W^s) and unstable (W^u) manifolds of the saddle type fixed point $\bar{\zeta}$, associated with the periodic motion, are defined as those sets of points in Σ which are, respectively, forward and backward asymptotic to the fixed point under iterates of map P :

$$W^s = \{ \zeta \in \Sigma \text{ (or } \in \Sigma^{t_0}) : P^n(\zeta) \rightarrow \bar{\zeta} \text{ as } n \rightarrow +\infty \} \quad (3.4.1)$$

$$W^u = \{ \zeta \in \Sigma \text{ (or } \in \Sigma^{t_0}) : P^n(\zeta) \rightarrow \bar{\zeta} \text{ as } n \rightarrow -\infty \} . \quad (3.4.2)$$

Using digital simulations, we can generate portions of these sets and examine when the stable and unstable manifolds intersect transversely which implies that there exists "Smale horseshoes" for P and that chaotic motions will exist in the system. Iterating two nearby points in the horseshoe set under the map P reveals that the points will diverge quickly. This sensitive dependence on initial conditions is characteristic of chaotic motions.

Figure 17 shows the frequency response of impact velocity at paper versus forcing period. At point A the motion begins to undergo a succession of period doubling or flip bifurcations, which eventually results in chaos. Simulations (see Figure 9) show that the period doubling bifurcations are supercritical. In Figure 9 we choose a fixed point which corresponds forcing frequency $\omega = 3.9$ for which the associated motion is chaotic. By digital simulations, we choose many initial points very near to the unstable fixed point and iterate the mapping forward to generate the unstable manifold and backward to generate the stable manifold as shown in Figure 18. It shows that the stable and unstable manifolds intersect transversely which implies the existence of horseshoes via the Smale-Birkhoff homoclinic theorem [39]. The map P is piecewise smooth, but discontinuous. The discontinuity is due to a degenerate, grazing type of impact at the backstop. Thus the stable and unstable manifolds are disconnected sets [35].

A Smale horseshoe is a complicated invariant set. It can be shown that the horseshoe is a Cantor set which contains the following: (a) a countable infinity of unstable periodic orbits including those of arbitrarily long periods, (b) an uncountable infinity of unstable,

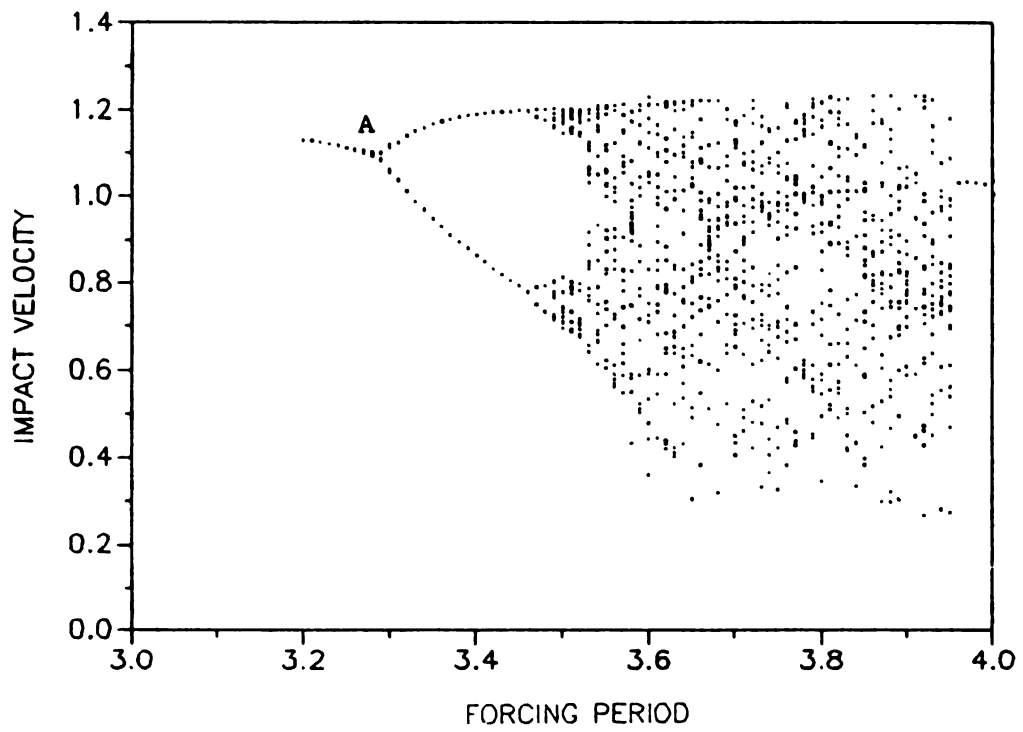


Figure 17. Frequency response.

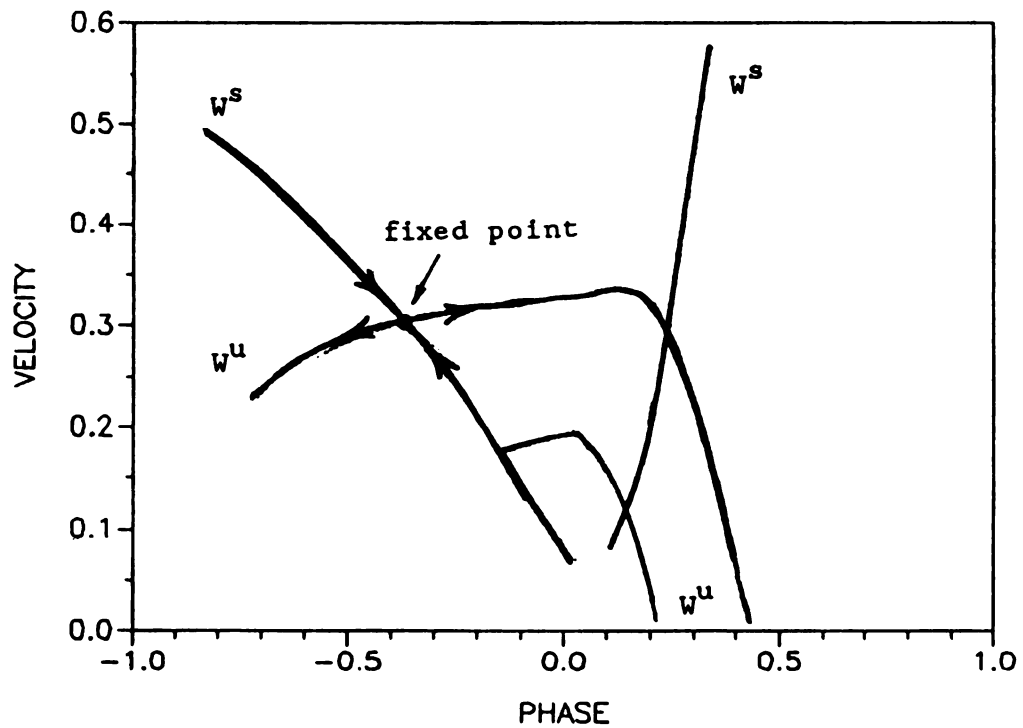


Figure 18. Intersection of the stable and unstable manifolds in Σ_1 (only the first few branches are depicted).

bounded, nonperiodic orbits, and (c) a dense orbit. The horseshoe is not attractive. It acts as a chaotic saddle point since most orbits approaching it eventually leave its neighborhood. Points near the horseshoe display an extremely sensitive dependence upon initial conditions. It does form the "heart" of the strange attractor, however, in that the motion may move from horseshoe to horseshoe indefinitely if no other attracting sets are nearby.

Points in the strange attractor on the Poincare section Σ appear to lie on a set of curves that resembles the unstable manifold. This is so since points near the horseshoe tend to converge towards the unstable manifold and be diverged along the unstable manifold. An attracting set containing horseshoes is referred to as a strange attracting set (see Guckenheimer and Holmes [39], Devaney [45], and Chillingworth [46] for details).

Using the Poincare section Σ_1 of equation (2.2.4), we can establish the existence of an attracting set in our system. Let the region $R = \{t, y | 0 \leq y \leq L\} \subset \Sigma_1$ in the cylindrical (T-periodic in t) Poincare section. If L is taken sufficiently large, then we can show that $P(R) \subset R$ as follows. The armature leaves the backstop with velocity $y_0 > 0$ at time t_0 and is excited by a half sine pulse to hit the paper with the velocity y_3 and t_3 . Using the time derivative of equation (3.1.3), we obtain

$$y_3 = e^{-\alpha_1(t_3-t_0)} \Omega_1 [A_0 \sinh(\Omega_1(t_3-t_0)) + B_0 \cosh(\Omega_1(t_3-t_0))]$$

$$\begin{aligned}
& -\alpha_1 e^{-\alpha_1(t_3-t_0)} [A_0 \cosh(\Omega_1(t_3-t_0)) + B_0 \sinh(\Omega_1(t_3-t_0))] \\
& + (\beta/2\Omega_1) \{ e^{(\Omega_1-\alpha_1)(t_3-t_1)} (e^{(\alpha_1-\Omega_1)D} + 1.0) [\omega/((\alpha_1-\Omega_1)^2 + \omega^2)] \\
& (\Omega_1-\alpha_1) + e^{-(\Omega_1+\alpha_1)(t_3-t_1)} (e^{(\alpha_1+\Omega_1)D} + 1.0) [\omega/((\alpha_1+\Omega_1)^2 + \omega^2)] \\
& (\alpha_1+\Omega_1) \} . \tag{3.4.3}
\end{aligned}$$

Since we assume that y_0 is sufficiently large, equation (3.4.3) can be simply written as

$$\begin{aligned}
y_3 &= y_0 e^{-\alpha_1(t_3-t_0)} \cosh(\Omega_1(t_3-t_0)) - y_0 \alpha_1 e^{-\alpha_1(t_3-t_0)} \\
& \sinh(\Omega_1(t_3-t_0))/\Omega_1 + C \tag{3.4.4}
\end{aligned}$$

where C represents the terms independent of y_0 in equation (3.4.3).

From equation (3.4.4) we obtain

$$y_3 < y_0 \cosh(\Omega_1(t_3-t_0)) + C . \tag{3.4.5}$$

After impacting with the paper, the armature leaves the paper with velocity y_4 at time t_4 . Since energy dissipation occurs during the impact, we have

$$-y_4 < y_3 \quad . \quad (3.4.6)$$

Using the time derivative of equation (3.1.4) we get the impact velocity y_5

$$y_5 = e^{-\alpha_1(t_5-t_4)} \Omega_1 [A_4 \sinh(\Omega_1(t_5-t_4)) + B_4 \cosh(\Omega_1(t_5-t_4))] - \alpha_1 e^{-\alpha_1(t_5-t_4)} [A_4 \cosh(\Omega_1(t_5-t_4)) + B_4 \sinh(\Omega_1(t_5-t_4))] \quad . \quad (3.4.7)$$

We then write

$$y_5 = y_4 e^{-\alpha_1(t_5-t_4)} \cosh(\Omega_1(t_5-t_4)) - y_4 \alpha_1 e^{-\alpha_1(t_3-t_0)} \sinh(\Omega_1(t_3-t_0))/\Omega_1 + C1 \quad (3.4.8)$$

and obtain

$$-y_5 < -y_4 \cosh(\Omega_1(t_5-t_4)) - C1 \quad . \quad (3.4.9)$$

Substituting equations (3.4.5) and (3.4.6) into equation (3.4.9) we get

$$-y_5 < y_0 \cosh(\Omega_1(t_3-t_0)) \cosh(\Omega_1(t_5-t_4)) + C \cosh(\Omega_1(t_5-t_4)) - C1. \quad (3.4.10)$$

During an impact with the backstop a simple impact rule is applied and equation (2.1.11), $r = b = -0.15$, is employed. Then the armature leaves the backstop with velocity y_6 .

$$y_6 = -ry_0 \cosh(\Omega_1(t_3 - t_0)) \cosh(\Omega_1(t_5 - t_4)) + rC \cosh(\Omega_1(t_5 - t_4)) + rC_1. \quad (3.4.11)$$

Taking y_0 is sufficiently large, from equation (3.1.3) and (3.1.4) the durations $t_3 - t_0$ and $t_5 - t_4$ must be small. Then we conclude

$$y_6 < y_0 \quad (3.4.12)$$

for y_0 large. Hence the motion is bounded and an attracting set must exist.

There are some criteria often used to detect chaotic motion, one of them consists of considering the power spectra of dynamic variables of the system [47]. When we have a stable periodic motion the power spectra is merely a sum of discrete peaks. Chaotic motion is characterized by the existence of a continuous spectrum without the existence of any random inputs or parameters. This method is often used in numerical experiments or directly in physical experiments. Another criterion for determining the existence of chaotic motion is connected with the main characteristic exponent of Lyapunov[48,49,50]. Lyapunov exponents, which are the average exponential rates of divergence or convergence of nearby orbits in phase space, can be used

to characterize the system response. Any bounded motion of a system containing at least one positive Lyapunov exponent is defined to be chaotic. All strange attractors in three dimensional space have the same spectral type, $(+,0,-)$: a positive exponent indicating the separation of trajectories within the attractor, a zero exponent for the motion along the orbit in time (Haken [51] has proven that at least one exponent vanishes if the trajectory of an attractor does not contain an equilibrium point), and a negative exponent for the contraction of nearby trajectories onto the attractor. The sum of the exponents is necessarily negative for a dissipative system and thus the phase space contains at least one attractor. A one dimensional map has a single exponent which is positive, negative or zero for chaotic, periodic, and marginally stable behavior, respectively. In a three dimensional continuous dissipative system, such as our printer model, the only possible spectral types for attractors, i.e., stable steady states, are: $(+,0,-)$, a strange attractor; $(0,0,-)$, a torus, or quasiperiodic, motion; $(0,-,-)$, a stable limit cycle; and $(-,-,-)$, an equilibrium point.

The algorithm for computing the Lyapunov spectrum from an equation of motion has been described in detail in Wolf et al. [49]. Lyapunov exponents are defined by the long-time evolution of the axes of an infinitesimal sphere of states. The sphere will become an ellipsoid due to the locally deforming nature of the flow. The i th one dimensional Lyapunov exponent is then defined in terms of the length of the ellipsoidal principal axis $p_i(t)$:

$$\lambda_1 = \lim_{t \rightarrow \infty} \log_2 \frac{p_1(t)}{p_1(0)} . \quad (3.4.13)$$

The phase space together with its tangent space is used to calculate Lyapunov exponents. A fiducial trajectory (the center of the sphere) is defined by the action of the nonlinear differential equations on some initial condition. Trajectories of points on the surface of the sphere are defined by the action of the linearized differential equations of motion on points infinitesimally separated from the fiducial trajectory. The principal axes are defined by the evolution via the linearized equations of an initially orthonormal vector frame anchored to the fiducial trajectory. However such a method is only applicable to continuous dynamic systems, since the linearized differential equations are not well defined at discontinuities. In our case the discontinuity occurs at impact with the backstop. Thus for our piecewise linear system, a discrete mapping will be used to calculate the Lyapunov exponent. Using the Poincare section Σ^{t_0} of equation (2.2.2) and the associated map P , we can calculate DP by following a procedure similar to that described in Chapter 3 for stability analysis. The DP is a composite map similar to DP of equation (3.2.4). However, in this case DP is more complicated since the associated orbits involve impacts that occur during the application of the driving pulse and impacts that do not occur during some forcing periods. The linearized map can be expressed as

$$\begin{bmatrix} \delta x_{n+1} \\ \delta y_{n+1} \end{bmatrix} = DP^n(X_0) \begin{bmatrix} \delta x_n \\ \delta y_n \end{bmatrix} \quad (3.4.14)$$

where X_0 represents an arbitrary initial condition, i.e., $X_0 = (x_0, y_0)$.

An orthonormal frame of principal axis vectors such as $((0,1), (1,0))$ is evolved by applying DP to each vector, i.e.,

$$\begin{bmatrix} \delta x_{n+1} \\ \delta y_{n+1} \end{bmatrix} = DP(X_n)DP(X_{n-1})\dots DP(X_0) \begin{bmatrix} 0 \\ 1 \end{bmatrix} \quad (3.4.15)$$

where $X_j = P(X_{j-1})$. Similarly equation (3.4.15) applies to the vector $(1,0)$. Lyapunov exponents μ can be computed from the growth (contraction) rate of the length of the first vector and the growth (contraction) rate of the projection of the second vector on the vector orthogonal to the first vector or from the eigenvalues of the long-time product matrix, DP^n , of the linearization of the map P , i.e.,

$$\mu_1 = \lim_{n \rightarrow \infty} \left(\frac{1}{n} \right) \log_2 |\lambda_1| \quad (3.4.16.)$$

where λ_1 is an eigenvalue of the linearized map $DP^n(X_0)$. However, the long time product matrix tends to become a singular matrix since all the columns in the matrix converge to large multiples of the eigenvector corresponding to the biggest eigenvalue of the matrix. Also, the magnitude of the current axis vector diverges (converges),

and the angular separation between the two vectors goes to zero as the axis vectors multiply DP. Gram-Schmidt reorthonormalization (GSR) is used to solve this problem.

In this dissertation the Lyapunov exponents are calculated as follows. At each iterate DP acts on the two unit axis vectors, e_1 and e_2 , and we construct the unit vector along the image of e_1 to be used as the first unit axis vector for the next iteration, i.e.,

$$e_1^{(j)} = \frac{DP(\zeta_{j-1}) e_1^{(j-1)}}{|DP(\zeta_{j-1}) e_1^{(j-1)}|} \quad (3.4.17)$$

where $P(\zeta_{j-1}) = \zeta_j$, ζ_0 is any initial condition we choose and j is the iteration number. The second axis vector for the next iterate is constructed by removing that component of the image of e_2 which is parallel the image of e_1 and then normalizing, i.e.,

$$e_2^{(j)} = \frac{DP(\zeta_{j-1}) e_2^{(j-1)} - \langle DP(\zeta_{j-1}) e_2^{(j-1)}, e_1^{(j)} \rangle e_1^{(j)}}{|DP(\zeta_{j-1}) e_2^{(j-1)} - \langle DP(\zeta_{j-1}) e_2^{(j-1)}, e_1^{(j)} \rangle e_1^{(j)}|} \quad (3.4.18)$$

where \langle , \rangle denotes the usual inner product. Then the Lyapunov exponent μ_1 is given by

$$\mu_1 = \lim_{n \rightarrow \infty} \left(\frac{1}{n} \right) \sum_{j=1}^n [\log_2 (\ell_1^j)] \quad (3.4.19)$$

where $i = 1, 2$ and $\ell_1^j = |\text{DP}(\zeta_{j-1}) e_1^{(j-1)}|$, $\ell_2^j = |\text{DP}(\zeta_{j-1}) e_2^{(j-1)}|$.

$\langle \text{DP}(\zeta_{j-1}) e_2^{(j-1)}, e_1^{(j)} \rangle e_1^{(j)}|$. The removal of components parallel to $e_1^{(j)}$ is required to compute μ_2 since without this step all vectors will simply approach the eigenvector associated with the largest eigenvalue and only μ_1 could be determined.

For the stable periodic motion the Lyapunov exponents can be directly calculated from the eigenvalues of the $\text{DP}(\bar{\zeta})$ evaluated at the stable fixed point $\bar{\zeta}$ since at an arbitrary initial condition DP will eventually approach the constant matrix which is equal to $\text{DP}(\bar{\zeta})$. Thus the Lyapunov exponents μ can be expressed as $\mu_1 = \log|\lambda_1|$, $\mu_2 =$

$\log|\lambda_2|$ where $\lambda_{1,2}$ are the eigenvalues of $\text{DP}(\bar{\zeta})$ for a two dimensional map. It is clear that the definition of Lyapunov exponent generalizes the idea of eigenvalue to give average linearized contraction and expansion of the system over the global regions of the phase space.

At the same parameter, chosen in this section above, $\omega = 3.9$, from digital simulations for the trajectory and the direct calculation for DP we determine the Lyapunov exponents for the strange attractor to be 1.14 and -5.10 for an arbitrary initial condition. The spectral type is $(-, +)$ for the map, and $(-, 0, +)$ for the flow. The zero component is suppressed for the map since time is "removed" by the map. Thus it shows that the associated motion at this parameter value is chaotic. For the forcing frequency $\omega = 3.3$ which is close to the

bifurcation point, the Lyapunov exponents are equal to -0.00155 and -4.3572. As we expected, one of Lyapunov exponents is nearly zero and the spectral type is $(-, -)$ for stable periodic motion. For the parameter value $\omega = 3.45$ the associated motion is stable motion with period $2T$ and the Lyapunov exponents are equal to -0.2068 and -3.15. It should be noted that even if a different initial condition is chosen, the average rate of expansion and contraction is of the same type and the same Lyapunov exponents will be obtained since the Lyapunov exponent is computed based on the long time behavior of a trajectory.

CHAPTER IV

A METHOD FOR THE IMPROVEMENT OF PERFORMANCE

4.1 An Open-Loop Control Strategy and Printer Performance Criteria

The control strategy which we propose to increase the operation speed utilizes the coil which in normal operation is excited by a current pulse producing a magnetic field opposed to that of the permanent magnet, thus releasing the armature. Immediately before firing, we propose that an inverted pulse be applied, here called the damping pulse, of opposite sense to the driving pulse. This aids the force of the permanent magnet and quickens settle-out of the armature. This is done in an open-loop fashion without requiring additional sensors or signal processing. A periodic full sine pulse as shown in Figure 19 will represent the forcing function, i.e., the current sent through the coil.

This control strategy is quite specific, it was chosen because of its simplicity and effectiveness. It may be tested on more complicated models and actual impact printers of the stored energy type.

It is important to note that the driving current pulses in actual printers are not generally periodic. Actual printers are operated under various "firing combinations", i.e., time lapses between input driving pulses are varied and are specified by a particular pattern of dots required to form the desired characters. General printer

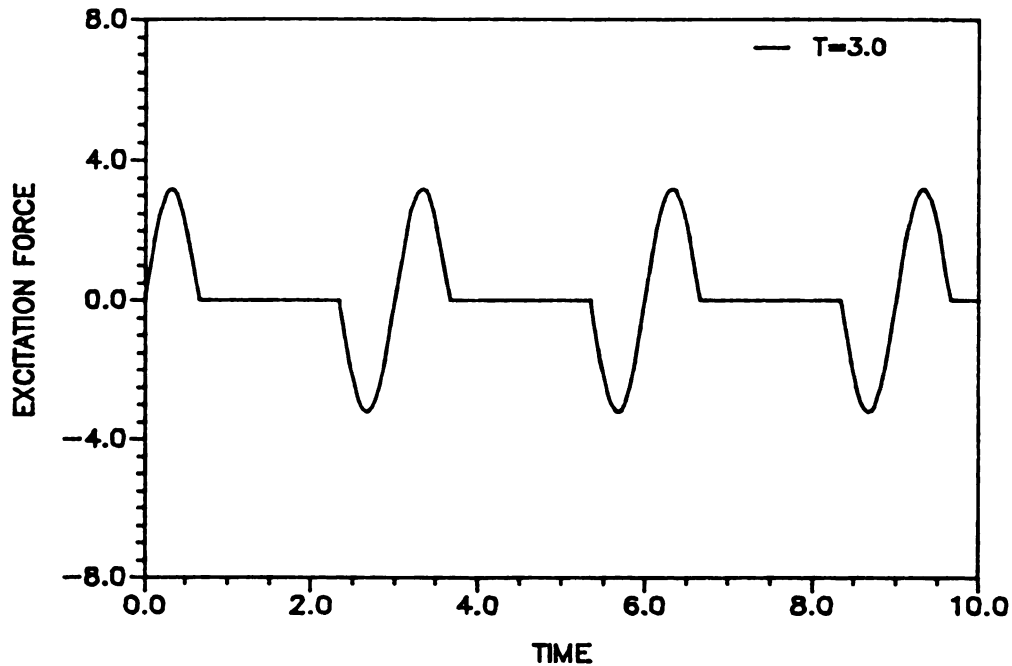


Figure 19 Periodic full sine pulses

performance criteria are established and are based on the requirement that acceptable print quality be achieved for an entire class of firing combinations with some minimum time lapse between pulses. This minimum period is typically the lowest period which provides acceptable steady state, i.e., periodic, operation. This requirement must also hold for all physically possible initial conditions which may be provided at the time of refiring. This condition is necessary since the print hammer must be fired before complete settle-out if the printer is to run at an increased operating speed.

Any control strategy, including ours, should thus satisfy the following three conditions in principle:

(a) Any initial conditions provided for refiring which result in acceptable print quality will continue to do so for all subsequent

firings. This implies that once a firing results in acceptable print quality, all subsequent refirings will result in acceptable print quality.

(b) Any initial conditions provided for refiring which do not result in acceptable print quality will be mapped in to the "acceptable print region" in a single iterate. This implies that although refiring may result in unacceptable print quality for a single dot, due to some disturbance, all subsequent refirings will result in acceptable print quality.

(c) When fired from rest the system must print an acceptable dot. This, along with (a), insures that the printer will perform satisfactorily from a "cold" start.

Conditions (a) and (b) will depend on the time elapsed from the previous pulse. Thus they must hold for all periods larger than the minimum acceptable operating period. Condition (c) depends on the model and is satisfied for printers which operate by requiring settle-out to be nearly complete at refiring. These conditions may be relaxed, they are "worst case" criteria.

We now present these criteria more formally. We begin with the criteria for periodic pulse inputs, this is the simplest case. The results are then extended, by a modification of the map P^{t_0} (written simply as P in this Chapter) to cases where the input pulses are non-periodic.

We assume that pulses do not occur until the hammer has left the paper. All reasonable driving periods will satisfy this condition since we assume that the printers will not be operated at periods

larger than the "buzz" printing speed in which the hammer never returns to the backstop.

Using (a), (b) and (c) with the map P we can establish and verify printer performance criteria for the periodic pulse case as follows.

Let D be the region in Poincare section Σ^{t_0} (equation (2.2.2)) which represents all initial conditions (x,y) which are physically possible at the time of the driving pulse application. Also, let Ω denote the subset of D which contains those initial conditions for refiring which result in acceptable print quality. Control strategies intended to improve the printer performance, for example by increasing the operating speed and/or extending stability ranges, must satisfy the following conditions in order to meet conditions (a), (b) and (c) above:

$$P(D) \subset \Omega \quad (4.1.1)$$

(this is equivalent to (b) above).

Then since $\Omega \subset D$ and $P(D) \subset \Omega$

$$P(\Omega) \subset \Omega \quad (4.1.2)$$

(this satisfies (a) above).

Also, if $(x,y) = (\bar{x},0)$ is the printer's rest position, then

$$(\bar{x}, 0) \in \Omega \quad (4.1.3)$$

(this satisfies (c) above).

The set Ω is referred to as a trapping region for P since (4.1.1) implies (4.1.2), i.e., (b) implies (a). Hence, since points in D will be mapped in to Ω in a single iterate, points in Ω will remain in Ω for all iterates. To satisfy (c), the printer rest position must be in the set Ω , i.e., (4.1.3) above; this is usually satisfied since normal printers operate such that settle-out is nearly complete at each driving pulse application. These conditions can be checked via simulation studies of a printer model.

Next, we establish criteria, similar to those above, for non-periodic inputs. Figure 20 shows a non-periodic pulse sequence as an example of the type of input to which the printer must respond. The first two pulses shown are assumed to be separated by the minimum allowable time lapse between pulses. Any pulses spaced closer than

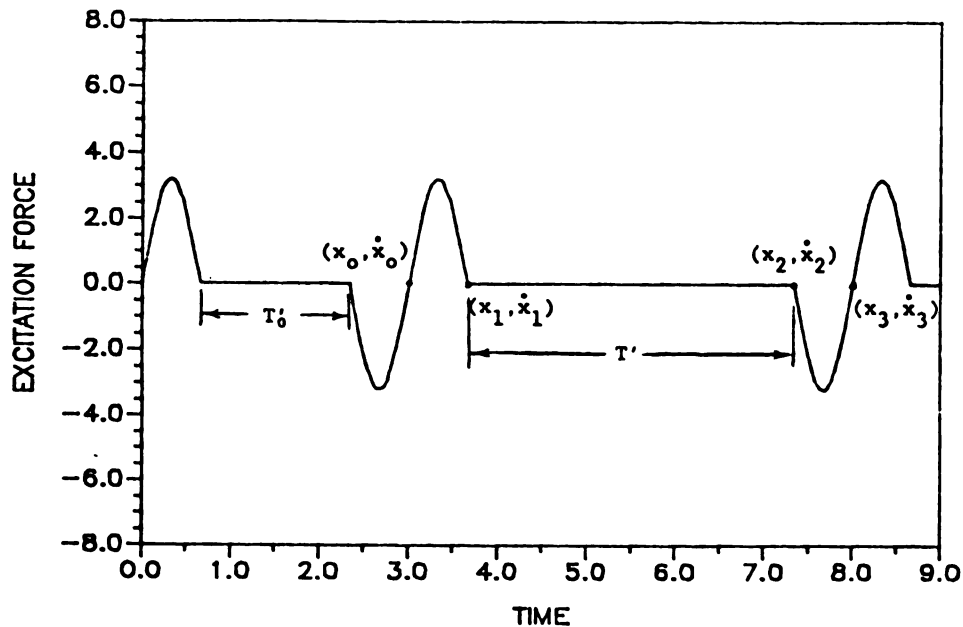


Figure 20 General firing combinations with full sine pulses

this will result in unacceptable print quality. The duration of the driving and damping pulses are assumed to be equal and are denoted as d ; this equality is not necessary but is chosen here for convenience. The time lapse between pulses is denoted T' and will have a range from the minimum value T'_0 to ∞ . We call the minimum period $T_0(-T'_0 + 2d)$. It will be convenient to think of a single pulse cycle as consisting of three portions in a particular order: 1) first, the driving pulse is fired which releases the armature, 2) then the unforced phase of the motion during which the hammer strikes the ribbon and paper and settle-out begins and, lastly, (3) the damping pulse is applied which facilitates settle-out, see Figure 21(a).

For each part of the cycle we can define a map which relates the final (x,y) values of that part to the (x,y) values at its beginning. Let PP denote the map

$$PP : (x_0, y_0) \rightarrow (x_1, y_1) \quad (4.1.4)$$

which takes the initial condition at the beginning of the cycle, i.e., at the start of the driving pulse and maps it to the (x,y) value at the time at which the pulse ceases, (x_1, y_1) . Similarly, let $PN_{T'}$ be the map

$$PN_{T'} : (x_1, y_1) \rightarrow (x_2, y_2) \quad (4.1.5)$$

governed by the unforced portion of the cycle. PN_T , determines where the point (x_1, y_1) will go after a time duration T' , during which the paper is struck and settle-out begins. We label this end-point (x_2, y_2) . Note that T' will vary from cycle to cycle. Finally we have a map PI which relates the initial settle-out point (x_2, y_2) to the a state (x_3, y_3) at which time refiring will occur;

$$PI : (x_2, y_2) \rightarrow (x_3, y_3). \quad (4.1.6)$$

Note that (x_0, y_0) and (x_3, y_3) are similar states. We cannot, however, use the usual notion of a Poincare map since the sampling of (x, y) states is irregular in time due to the non-periodic nature of the input. The composite map, depicted in Figure 21(b), is:

$$P_T = PI \circ PN_T \circ PP : (x_0, y_0) \rightarrow (x_3, y_3). \quad (4.1.7)$$

This will be quite useful for our analysis. Note that for a given printer, P_T is a one-parameter family of maps since T' may take on any value $T' \geq T'_0$ during operation.

In order to meet the performance criteria given above the following must hold for P_T :

$$1) P_T(x, y) \in \Omega \text{ for all } (x, y) \in D \text{ and all } T' \geq T'_0$$

(satisfies conditions (a) and (b))

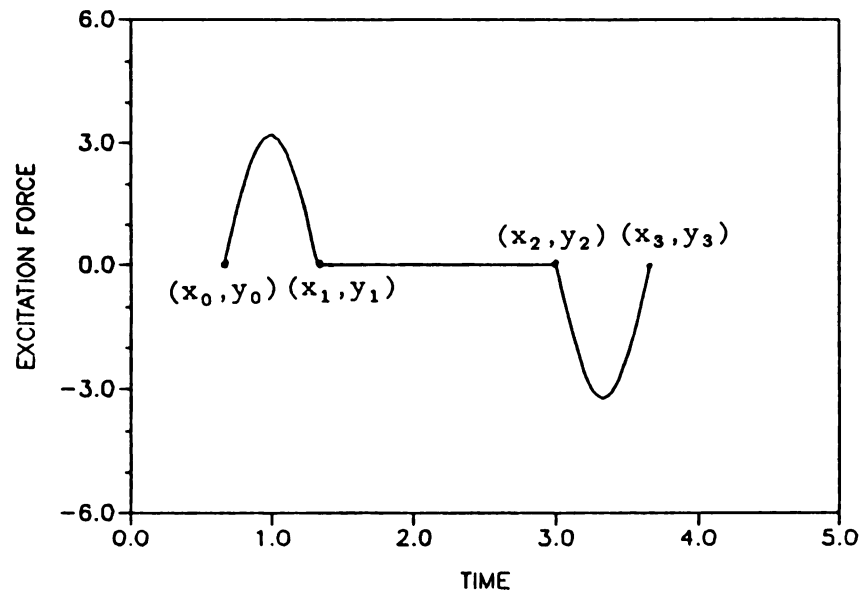


Figure 21(a). A driving cycle.

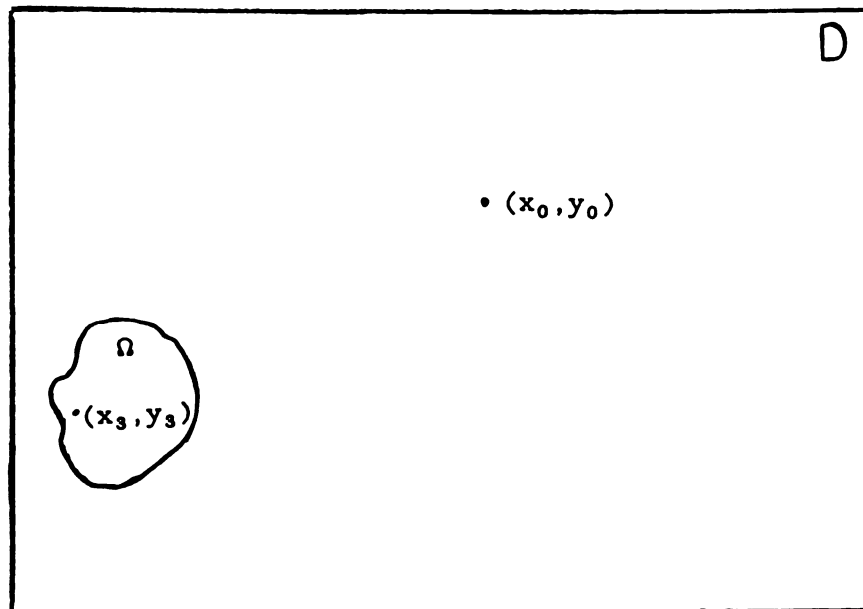


Figure 21(b). Composite map in Σ .

- ii) $(\bar{x}, 0) \in \Omega$ where $(\bar{x}, 0)$ is the rest position of the armature
(satisfies (c)).

Note that i) implies $P_T(x, y) \in \Omega$ for all $(x, y) \in \Omega$ so that (a) is satisfied by i) immediately above.

The printer must be able to respond to a wide variety of pulse timing combinations and disturbances. The smallest period, T_0 , to satisfy i) above is the period which determines the maximum printer speed for reliable operation, i.e.,

$$T_0 = \inf\{T : P_T(x, y) \in \Omega \text{ for all } (x, y) \in D \text{ and all } T' > T_0 \text{ with } (\bar{x}, 0) \in \Omega\}.$$

It should be noted that one may be able to find some period which is lower than T_0 for which the printer will operate satisfactorily in a periodic manner.

In the next two sections we test our control method and our performance criteria on the two single degree of freedom printer models, Hendriks' model and our piecewise linear model. For each we establish the maximum speed of operation by utilizing the printer performance criteria for both the periodic and the non-periodic cases. It is shown that print forces are less varied for the controlled system than are the uncontrolled system, and the printer performance criteria are satisfied for the controlled system with smaller minimum T . This implies that the proposed control strategy indeed results in an increase in operating speed.

4.2 Simulations and Results : Periodic Input

In this section we demonstrate the usefulness of the damping pulse in aiding settle-out for the case when the printer is operated by a periodic train of pulses. Hendriks [10] and the author (Chapter 3) have shown that chaotic motions of impact print hammers exist over wide ranges of parameter values for periodic inputs. By using the iterates of the Poincare map P , i.e., plotting all points which belong to Poincare section Σ^{t_0} , it has been found that as the forcing period is increased, the steady-state phase points converge towards to the rest position of the system. The points in Σ^{t_0} remain within a finite, and decreasingly small region near $(\bar{x}, 0)$ as T is increased. Since these steady state phase points represent the initial conditions for refiring, we can tell that the corresponding print forces are also within some finite range. If the print forces are adequate, then the phase points must belong to the acceptable print region Ω .

Using digital simulations of our model, we have plotted the impact velocity at the paper position and the maximum paper force versus forcing period by setting the print hammer in the rest position and exciting the print hammer by periodic half sine pulses and periodic full sine pulses respectively. The results are discussed below.

In the following; (a) denotes the system excited by periodic half sine pulses and (b) denotes the system excited by periodic full sine pulses, all started from the rest position. Figures 22 (a) and (b)

show plots of the paper impact velocity versus forcing period for our model. It is observed that chaotic motions (represented by steady-states with wide variations) exist over a wide range of the forcing periods. After implementation of our control strategy, the impact velocities are bounded within a smaller variation and converge to the velocity corresponding to the firing at rest position more quickly. Figures 23 (a) and (b) show plots of maximum print force versus forcing period. The dotted line to which the print forces converge represents the print force due to refiring from the rest position which is, of course, acceptable. The range of acceptable print forces is indicated in the figure by dashed lines. Thus from Figures 23 (a) and (b) it is seen that the system with periodic full sine pulses has a wider operation range with acceptable print quality than does the system with periodic half sine pulses. This shows the advantage of the proposed control strategy.

In order to investigate the effectiveness of this control strategy on actual impact printers, we also simulated Hendriks' model [10], which is more complicated than ours and may more accurately characterize the dynamics of impact printers. The results are shown in Figures 24 (a), (b) and 25 (a), (b) which show plots of the paper impact velocity and the maximum print force versus forcing period respectively. Similar to Figures 22 (a) and 23 (a), the impact velocities and maximum print forces in Figures 24 (a) and 25 (a) have a wide distribution, many of which are unacceptable. However, Figures 24 (b) and 25 (b) show that chaotic motions are less prevalent and that stable periodic motion with period T or period $2T$ are common, and that maximum print forces are generally adequate. This implies that

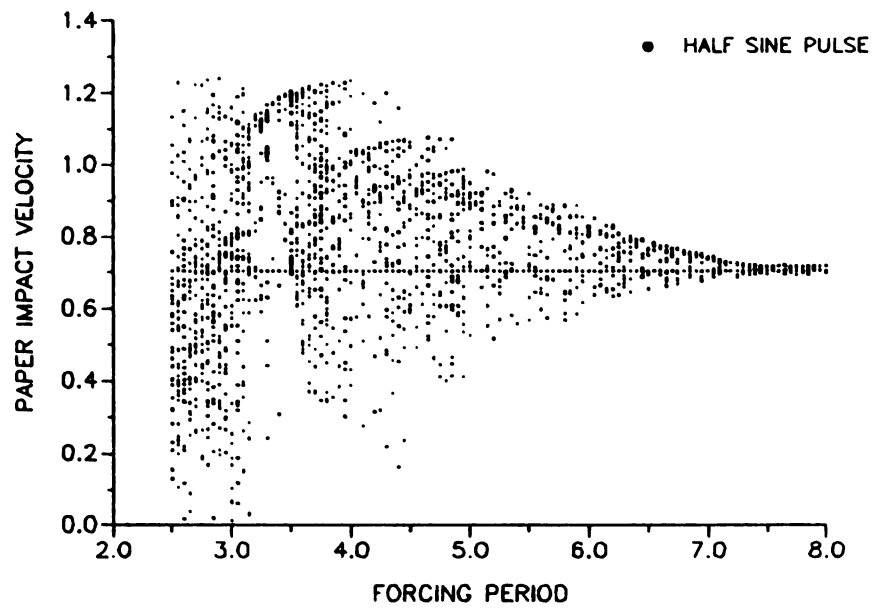


Figure 22(a) Frequency response for periodic half sine pulses
(piecewise linear model)

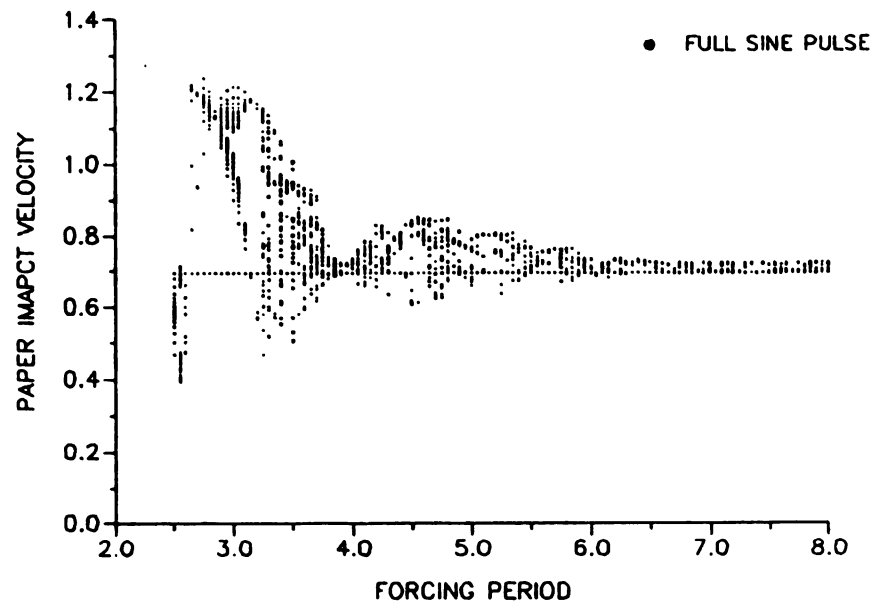


Figure 22(b) Frequency response for periodic full sine pulses
(piecewise linear model)

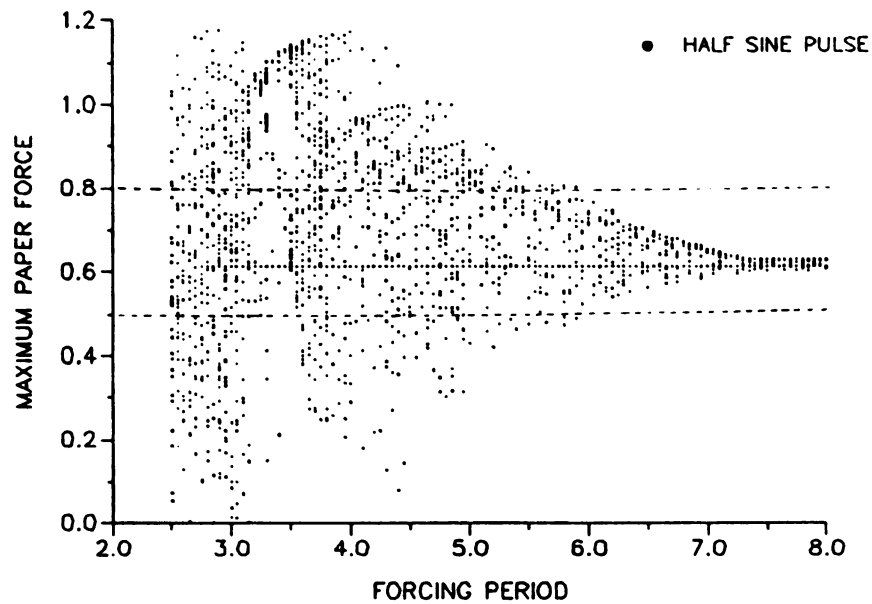


Figure 23(a) Frequency response for periodic half sine pulses
(piecewise linear model)

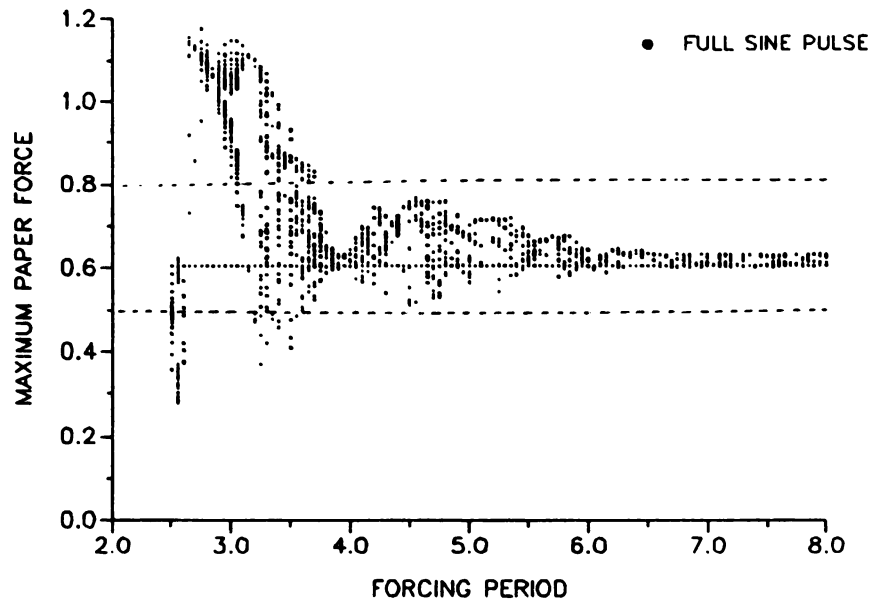


Figure 23(b) Frequency response for periodic full sine pulses
(piecewise linear model)

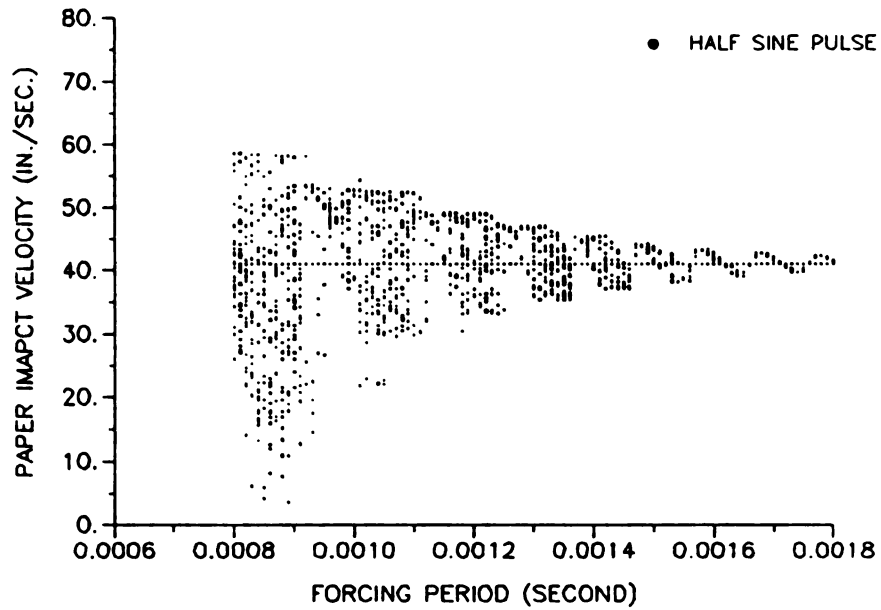


Figure 24(a) Frequency response for periodic half sine pulses
(Hendriks' model [10])

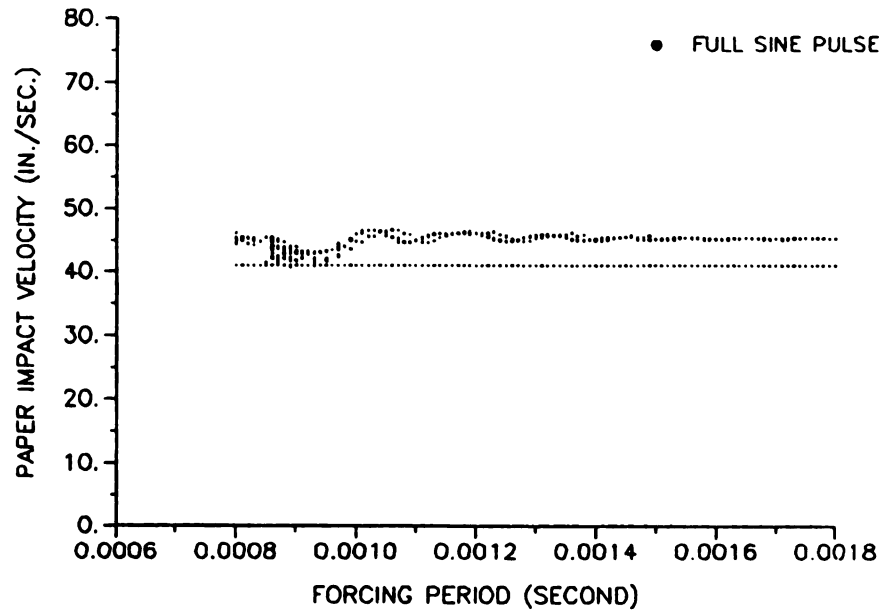


Figure 24(b) Frequency response for periodic full sine pulses
(Hendriks' model [10])



Figure 25(a) Frequency response for periodic half sine pulses
(Hendriks' model [10])

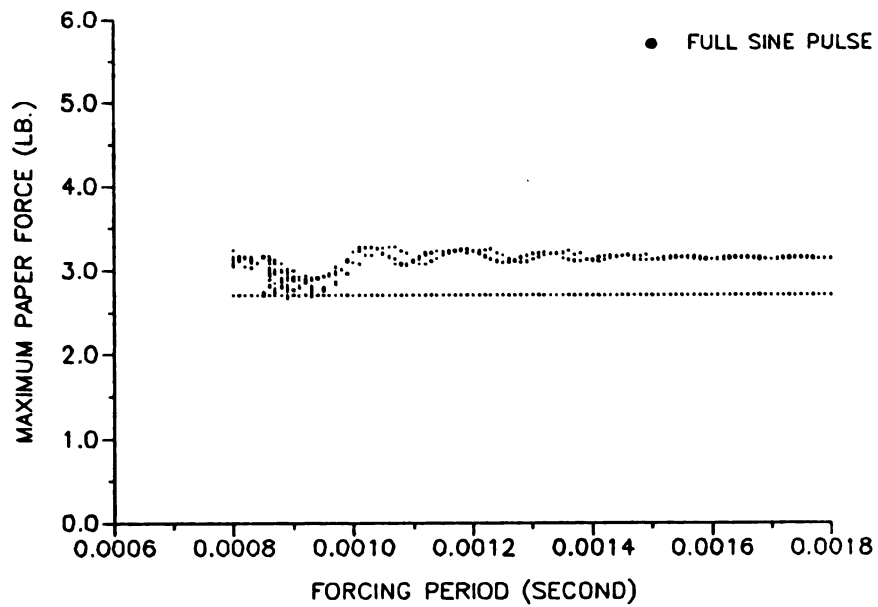


Figure 25(b) Frequency response for periodic full sine pulses
(Hendriks' model [10])

the operation frequency can be significantly increased using our control strategy.

The above indicates that printers operating in a periodic fashion can be improved. To address the same issue for more realistic, and quite arbitrary, firing combinations we turn to the proposed printer performance criteria.

4.3 Simulations and Result: General Firing Combinations

In this section we show that , based on the printer performance criteria, printers with the proposed control can be operated at higher speeds under arbitrary combinations of firing pulses with some minimum time lapse between pulses.

Actual printers are first fired from the rest position with the settle-out time sufficient for the armature to return very near to the rest position, then subsequent refiring results in acceptable print quality. However, due to a disturbance, such as noise or vibrations of the supporting structure, the refiring position may be far away from the rest position and unacceptable print quality occurs. This also occurs if the printer is refired too quickly. The printer performance criteria above were established to meet the requirement that acceptable print quality be achieved under disturbance and firing combinations.

First, we find the acceptable print region Ω . In this dissertation, we assumed that the region D in Poincare section Σ^{t_0} ,

which represents all possible initial conditions provided for refiring, is between 0.5 and -1.0 in velocity and between 0.2 and 0.8 in displacement. The displacement limits say that disturbance may allow the armature to be away from the rest position but that the system shall not refire while in contact with paper. The limited values of velocity that we choose here are based on the phase portraits obtained by simulations in previous chapter which indicate reasonable bounds for the velocity. The region D can be easily enlarged, doing so does not affect our results significantly. Digital simulations were run by firing a fine grid of initial conditions in D. This drives the armature to strike the paper the maximum paper deflection can be measured. The maximum print force for each firing can be derived from the maximum paper deflection. The acceptable print region is indicated in Figure 26. It is formed by

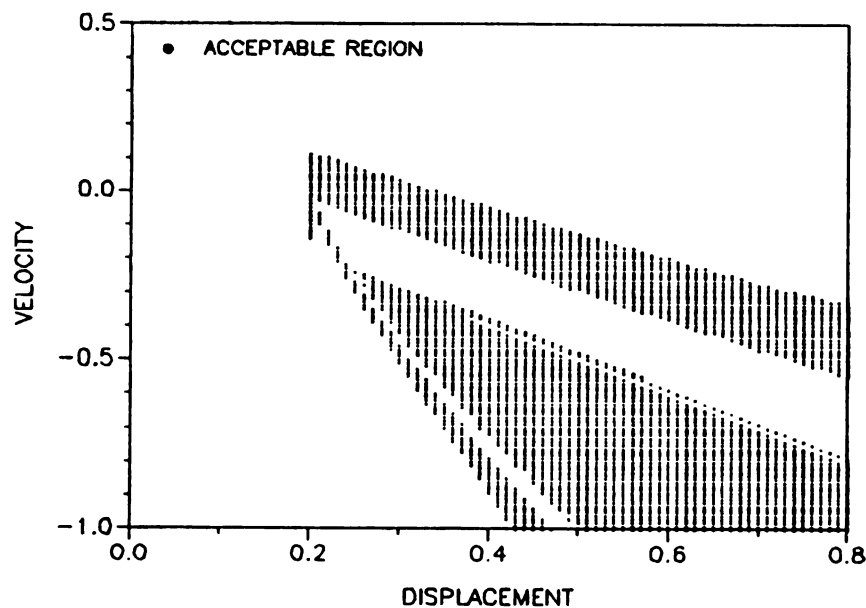


Figure 26 Acceptable region Ω

recording the initial conditions which result in acceptable print, i.e., the maximum print force is in the assumed range 0.5-0.8. (It is known that firing the armature from rest always results in a good dot on the paper. Thus we assume that the acceptable peak print forces are in a region which has some variation around the maximum print force which results from firing the armature from rest.) It should be noted that Ω is independent of the forcing period, T , if T is large enough so the refiring does not occur before the hammer leaves the paper.

Next, we search for the minimum period T_0 for which the corresponding map P_{T_0} satisfies condition (4.1.1). At first we begin with a large period T which consists of the driving pulse, the unforced portion T' which is long enough so that settle-out is nearly complete and the damping pulse. By digital simulations we check to see if this forcing cycle will take every initial condition in D into the acceptable region Ω or not. If it does, then we decrease this forcing period, i.e., decrease the duration of the unforced portion, T' , and recheck. The above procedure is repeated until one of the initial conditions is not taken into the acceptable region Ω by the forcing cycle. We then define the previous forcing cycle, which takes all initial conditions from D into Ω , to be the minimum period T_0 .

Using this simulation-based procedure, we obtain the minimum period T_0 and can be certain that for all forcing periods T larger than T_0 condition (4.1.5) will be satisfied. Figure 27 shows that the initial conditions in D are mapped into Ω with the minimum period T_0 which is

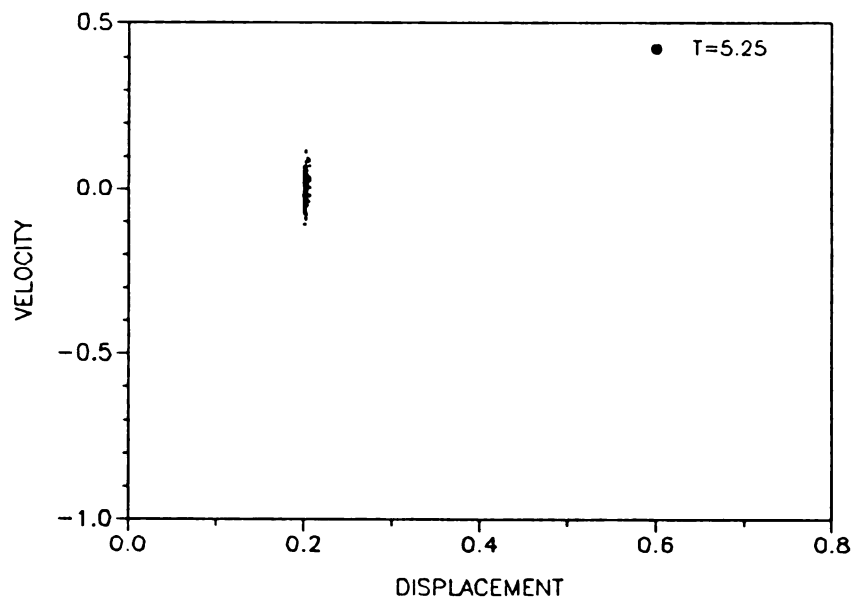


Figure 27. Initial condition of $P(D) \subset \Omega$, $T=5.25$

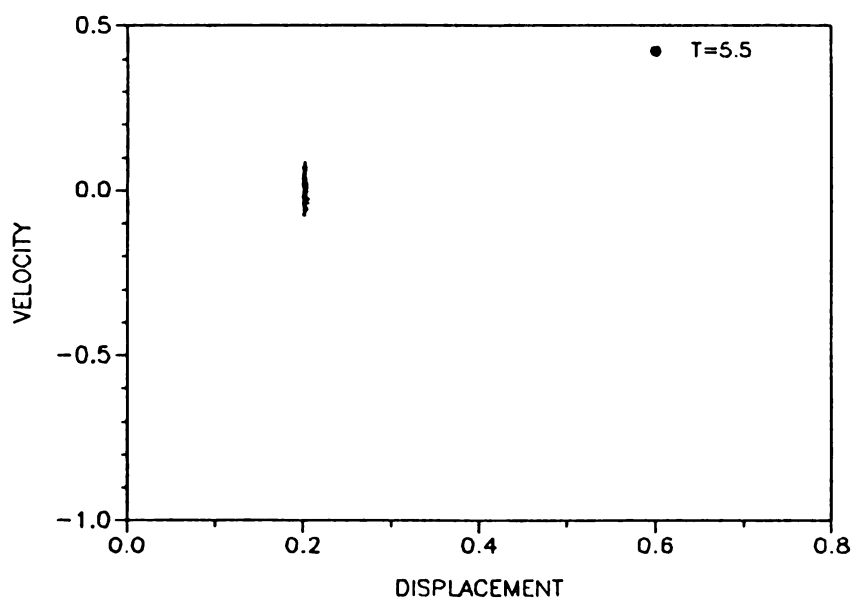


Figure 28. Initial condition of $P(D) \subset \Omega$, $T=5.5$

found to be equal to 5.25 for our model. Initial conditions in D are mapped into Ω with forcing periods larger than T_0 , $T = 5.5$ is given as an example in Figure 28. As expected, the longer the forcing period is, the closer the initial conditions are mapped to rest position. By using a searching method similar to the one described above it was determined that the minimum driving period for the uncontrolled system was $T_0 = 6.5$. Thus an increase in speed of approximately 20% is achieved without using feedback.

The unforced portion of a cycle, for the uncontrolled system, determines if there is sufficient time for the armature to reach the acceptable region or not. If the forcing period T is decreased, i.e., the unforced portion T' is decreased, the armature will not always reach the acceptable region within the time T' and the printer performance is unsatisfactory. However, by introducing the damping pulse, the system is forced into the acceptable region more rapidly and the printer performance criteria can be satisfied at higher operating speeds.

CHAPTER V

DISCUSSION AND CONCLUSIONS

In this dissertation we have shown that a simplified piecewise linear model of a stored energy impact printer can predict the same qualitative behavior as that of a more complicated and realistic model [10]. For actual impact print hammers the armature and the driving spring act as a cantilever beam with nonlinear boundary conditions. In Moon and Shaw [52] and Shaw [53] it has been shown that a single mode model of an elastic beam with one sided amplitude constraint can provide good overall qualitative information about actual physical system. This was done by comparing experimental results of the actual system with theoretical and digital simulation results of the single mode model which is piecewise linear in nature. Also, if the stiffness ratio of the driving spring and armature is small, i.e. the stiffness coefficient of the driving spring is small, the armature acts nearly as a rigid body. By considering the location of the center of rotation of the armature, the effects of higher frequency modes can be eliminated [8,9]. From the above we may conclude that using a single degree-of-freedom piecewise linear model in this dissertation is acceptable.

If a complicated many degrees-of -freedom model is developed, simulation studies of such a system are significantly more difficult since one must explore the responses of the system for several parameter values over wide ranges of realistic initial conditions. In

nonlinear systems there may exist many possible steady state motions at a given set of parameter values and the steady state is dependent on initial conditions. Different initial conditions may lead to completely different asymptotic behavior. In some regions, a small disturbance may cause the motion to change dramatically. Using the simple, one-degree-of-freedom, piecewise linear model we were able to thoroughly explore the stability regions and predict the qualitative behavior over a wide range of parameter values.

From the results in this thesis, it is seen that our model mimics Hendriks' model very well. It also allows us to perform existence and stability analyses for periodic hammer responses. Stable and unstable periodic motions, their bifurcation points, and chaotic motions were found to exist in our model and stability regions were explored. It was shown that chaotic motions exist over a wide range of forcing periods T . As the forcing period T is increased, the strange attractor associated with a chaotic motion becomes smaller. The chaotic dynamics of the system are discussed in detail.

In addition, the influence of various parameters on the performance have been discussed. It has been shown that one can improve the speed of the impact printer by increasing the damping of the backstop, possibly by changing material, or by increasing the preload during settle-out phase, possibly by employing a changing magnetic field. The use of preload to suppress vibrations at low amplitudes applies to other mechanical systems as well.

We have devised a control strategy based on the fact that the actual impact printers are operated under various "firing combinations", i.e., time lapses between input pulses are varied and

depend on the separation between dots which form the desired characters. This open-loop control method helps the system to nearly completely "settle-out" at the backstop in very short time so that the subsequent refiring can take place more quickly, thus significantly increasing the operating speed of current impact printers without much additional cost. Since actual printers are operated under various firing combinations, the printer performance criteria are set based on the requirement that acceptable print be achieved for a class of firing combinations with some minimum period T_0 . Using the map P_T and digital simulations one can verify these printer performance criteria.

The resonance curves in Figure 9 which were generated from the analysis may be useful in the design of systems with periodic input. In periodic impact printing, the most efficient printing mode is stable "resonant printing" [10] in which the pulse acts while the hammer is on the rise after the first impact with the backstop. In such a case the resonance curves are useful. However, they show "resonant" printing to be impractical for our print model because the range of stable resonant motion is very small. Also, actual impact print hammers are excited nonperiodically.

The printer performance criteria indicated that the minimum driving period for the uncontrolled system was $T_0 = 6.5$. There exists a stable region for periodic operation from $T = 3.95$ to $T = 4.0$. If the space between potential dots to be printed is constant, the driving period may possibly be decreased to a period in the range $3.95 < T < 4.0$ as follows. A sequence of consecutive dots will settle into the resonant printing mode. If one or more dots is then to be

skipped, the lapse between dots will be nT , with $n \geq 2$, which is larger than 6.5. Thus the next dot will be acceptable. However, transient motion will affect the print quality of subsequent dots. Further tests on this idea are needed before it is judged to be an acceptable operating mode.

Limitations for the proposed control may exist due to the saturation of forces on the armature in the magnetic field, heat generation, increased energy consumption, more impacts with backstop causing increased wear, and fatigue life. Further study is needed regarding these issues.

The control strategy discussed in this thesis is quite specific. It is chosen because of its simplicity and effectiveness. It may be tested on more complicated models and, preferably, on actual impact printers.

The printer performance criteria, however, are quite general and are applicable to systems with more degrees of freedom and complexity, including those with feedback controllers. The sets D and Ω and the various maps can be extended in a straightforward manner to higher dimensions. In fact, such criteria may be useful for other systems which must perform satisfactorily when subjected to irregularly timed pulses.

Impacting piecewise linear models, for example [23-35], have many applications in mechanical systems. In this dissertation we studied a piecewise linear model with nonharmonic periodic and nonperiodic excitation with a goal of providing the overall qualitative behavior of impact print hammers of the stored energy type. We hope this study has provided some contribution to the understanding of the dynamic

response of impact print hammers and to the improvement of impact printer performance. Also, the results may be applicable to other systems subjected to pulse inputs. In particular, the area of random pulse inputs could be treated using ideas similar to those of Chapter 4.

LIST OF REFERENCES

LIST OF REFERENCES

- [1] T.Y. Nickel and F.J. Kania, "Print Technology in IBM," IBM Journal of Research and Development Vol. 25, No 5, pp. 755-765 Sept., 1981
- [2] W.G. Spruth, "Printing Technologies," Computer and Graphics Vol. 7, No. 1, pp. 51-57, 1983
- [3] R.A. Myers and J.C. Tamulis, "Introduction to Topical Issues on Non-Impact printing Technologies," IBM Journal of Research and Development Vol. 28, No 3, pp. 234-240, May 1984
- [4] E.L. Lucente, "Preface," IBM Journal of Research and Development Vol. 28, No 3, pp. 233, May 1984
- [5] James Shero, "Wire-Matrix Impact Printers: Three types of Impact Technology," Computer Technology Review Vol. 4, pp. 185-188, summer 1984
- [6] A. Watanabe, H. Ando, and Y. Ohmori, "A Study for the Design of a New Mechanism of Wire Dot Print Head," The Transactions of the IECE of Japan Vol. 65, no 7. July 1982
- [7] F.W. Dauer, "Impact Printing," IEEE Transactions on Electronic Computers vol. 15, pp. 794-798, 1966
- [8] H.C. Wang and S.A. Hall, "Paper-Function Model for Wire-Matrix Printing," Proceedings of the Society for Information Display Vol. 24, 794-798, 1966
- [9] W.J. Yang, G.C. Chen, T.Z. Chen, W.C. Kang, G.Y. Yen, and M.J. Wirn, "A Study for the Design of the Motion of the Dot-Matrix Impact Printer Head," Electronics Research and Service Organization, Industrial Technology Research Institute, Taiwan, ROC, 1985
- [10] F. Hendriks, "Bounce and Chaotic Motion in Impact Print Hammers," IBM Journal of Research and Development Vol. 27, No 3, pp. 270-280, May 1983
- [11] S.H. Hall, "Literature Survey on Hammer Control," IBM Research, Eastview, New York, 1985
- [12] A.B. Carson and M.j. Tuzo, "Drive Circuit for Printing Head," U.S. Patent No. 4162131, July, 1979

- [13] N. Blom and J.T. Wor, "Printer, Provided with an Impact Device Comprising a Transducer," U.S. Patent No. 4192230, March, 1980
- [14] G.B. Barrus and J. Matula, "Printer Having Variable Hammer Release Drive," U.S. Patent No. 4280404, July, 1981
- [15] A.B. Carson and S.C. Harris, "Driving Force Control System for Impact Printer," U.S. Patent No. 4333398, June, 1982
- [16] U. Heider, "Impact Printing Device with an Improved Print Hammer," U.S. Patent No. 4429342, January, 1984
- [17] S. Wen, "Printer Hammer Settling Device," IBM Technical Disclosure Bulletin Vol. 27, pp. 2573-2574, 1984
- [18] O. Suzuki and K. Nakamura, "Dot Matrix Print Head," U.S. Patent No. 4428691, January, 1984
- [19] M. Isobe, H. Kikuchi, M. Teshima, T. Kodama, Sakura, M. Iwama, and Yokosuka, "Printer Head" , U.S Patent No. 4433926, February, 1984
- [20] K. Asano, Musashino, T. Kondo, and A. Sakaida, "Print Head for a Dot Matrix Printer, U.S. Patent No. 4389128, June, 1983
- [21] K. Asano, Musashino, T. Kondo, and S. Mizuno, "Print-Head of a Dot-Printer, U.S. Patent No. 4411538, October, 1983
- [22] C.C. Chiu, W.C. Kang, and T.J. Chen, "Multiwires Dot Matrix Impact Print Head," Patent, Electronics Research and Service Organization, Industrial Technology Research Institute, Taiwan, ROC, 1985
- [23] S.F. Masri and T.K. Caughey, "On the Stability of the Impact Damper," ASME Journal of Applied Mechanics Vol. 33, pp. 586-592, 1966
- [24] M. Senator, "Existence and Stability of Periodic Motions of a Harmonically Forced Impacting System," Journal of the Acoustical Society of America Vol. 47, pp. 1390-1397, 1970
- [25] P.J. Holmes, "The Dynamics of Repeated Impacts with a Sinusoidally Vibrating Table," Journal of Sound and Vibration Vol. 84, pp. 173-189, 1982
- [26] S.W. Shaw and P.J. Holmes, "A Periodically Forced Piecewise Linear Oscillator," Journal of Sound and Vibration Vol. 90, pp. 129-155, 1983
- [27] S.W. Shaw and P.J. Holmes, "A Periodically Forced Impact Oscillator with Large Dissipation," ASME Journal of Applied Mechanics Vol. 50, pp. 849-857, 1983

- [28] S.W. Shaw, "The Dynamics of a Harmonically Excited System Having Rigid Amplitude Constraints, Part I: Subharmonic Motions and Local Bifurcations," ASME Journal of Applied Mechanics, Vol. 52, pp. 453-458, 1985
- [29] S.W. Shaw, "The Dynamics of a Harmonically Excited System Having Rigid Amplitude Constraints, Part II: Chaotic Motions and Global Bifurcations," ASME Journal of Applied Mechanics, Vol. 52, pp. 459-464, 1985
- [30] S.W. Shaw, "On the Dynamic Response of a System with Dry Friction," Journal of Sound and Vibration, Vol. 108, pp. 305-325, 1986
- [31] M.S. Heiman, P.J. Sherman, and A.K. Bajaj, "On the Dynamics and Stability of an Inclined Impact Pair," Preprint, School of Mechanical Engineering, Purdue University, 1986
- [32] C.N. Bapat and S. Sankar, "Single Unit Impact Damper in Free and Forced Vibration," Journal of Sound and Vibration, Vol 99, pp. 85-94, 1985
- [33] G.S. Whitson, "The Vibro-Impact Response of a Harmonically Excited and Preloaded One-Dimensional Linear Oscillator," Journal of Sound and Vibration, Vol. 115, pp. 303-319, 1987
- [34] G.S. Whitson, "The Global Dynamics of a Vibro-Impacting Linear Oscillator," to appear in Journal of Sound and Vibration.
- [35] G.S. Whitson, "Singularity Structure in Vibro-Impact Dynamics," Manuscript.
- [36] M. Vidyasagar, Nonlinear System Analysis, Prentice-Hall, Englewood Cliffe, New Jersey, 1978
- [37] M.W. Hirsch and S. Smale, Differential Equations. Dynamical Systems, and Linear Algebra, Academic Press, New York, 1974
- [38] P.J. Holmes, "A nonlinear System with a Strange Attractor," Philosophical Transactions of the Royal Society London A, Vol. 292, PP. 419-448, 1979
- [39] J. Guckenheimer and P. Holmes, Nonlinear Oscillations. Dynamical System and Bifurcations of Vector Fields, Applied Mathematical Sciences, Vol. 42, Springer Verger, New York, 1983
- [40] P. Hartman, Ordinary Differential Equations, Wiley, New York, 1964
- [41] S.N. Chow and J.K. Hale, Methods of Bifurcation Theory, Springer Verger. New York, 1981
- [42] J. Carr, Applicatioon of Center Manifold Theory, Applied Mathematical Science No. 35, Springer Verge, New York 1981

- [43] M. Feigenbaum, "Quantitative Universality for a Class of Nonlinear Transformations," Journal of Statistical Physics, Vol. 19, pp. 15-52, 1979
- [44] "IMSL Library Reference Manual", by IMSL Inc., 1979
- [45] R.L. Devaney, A Introduction to Chaotic Dynamical Systems, Benjamin-Cummings, California, 1987
- [46] D.R.J. Chillingworth, Differential Topology with a View to Applications, Pitman Press, London, 1976
- [47] K. Tomita, "Periodically Forced Nonlinear Oscillators," in Chaos, Princeton University Press, Princeton, New Jersey, 1986
- [48] A.J. Lichtenberg and M.A. Liberman, Regular and Stochastic Motion, Applied Mathematical Sciences, Vol. 38, Springer Verge, New York, 1983
- [49] A. Wolf, J.B. Swinney and J.A. Vastano, "Determining Lyapunov Exponents form a Time serious," Physica 16 D, pp. 285-317
- [50] P. Collet and J.P. Eckmann, Iterated Maps on the Interval as Dynamical Systems, Progress in Physics, Vol. 1, Birkhauser, Boston, Massachusetts, 1980
- [51] F. Haken, "A Least One Lyapunov Exponent Vanishes if the Trajectory of an Attractor Does Not Contain a Fixed Point," Physics Letters, Vol. 94A , pp. 71-72, 1983
- [52] F.C. Moon and S.W. Shaw, "Chaotic Vibration of a Beam with Nonlinear Boundary Conditions," International Journal of Nonlinear Mechanics, Vol. 18, pp. 465-477, 1983
- [53] S.W. Shaw, "Forced Vibrations of a Beam with One-sided Constraint: Theory and Experiment," Journal of Sound and Vibration, Vol.99, pp. 199-212, 1985